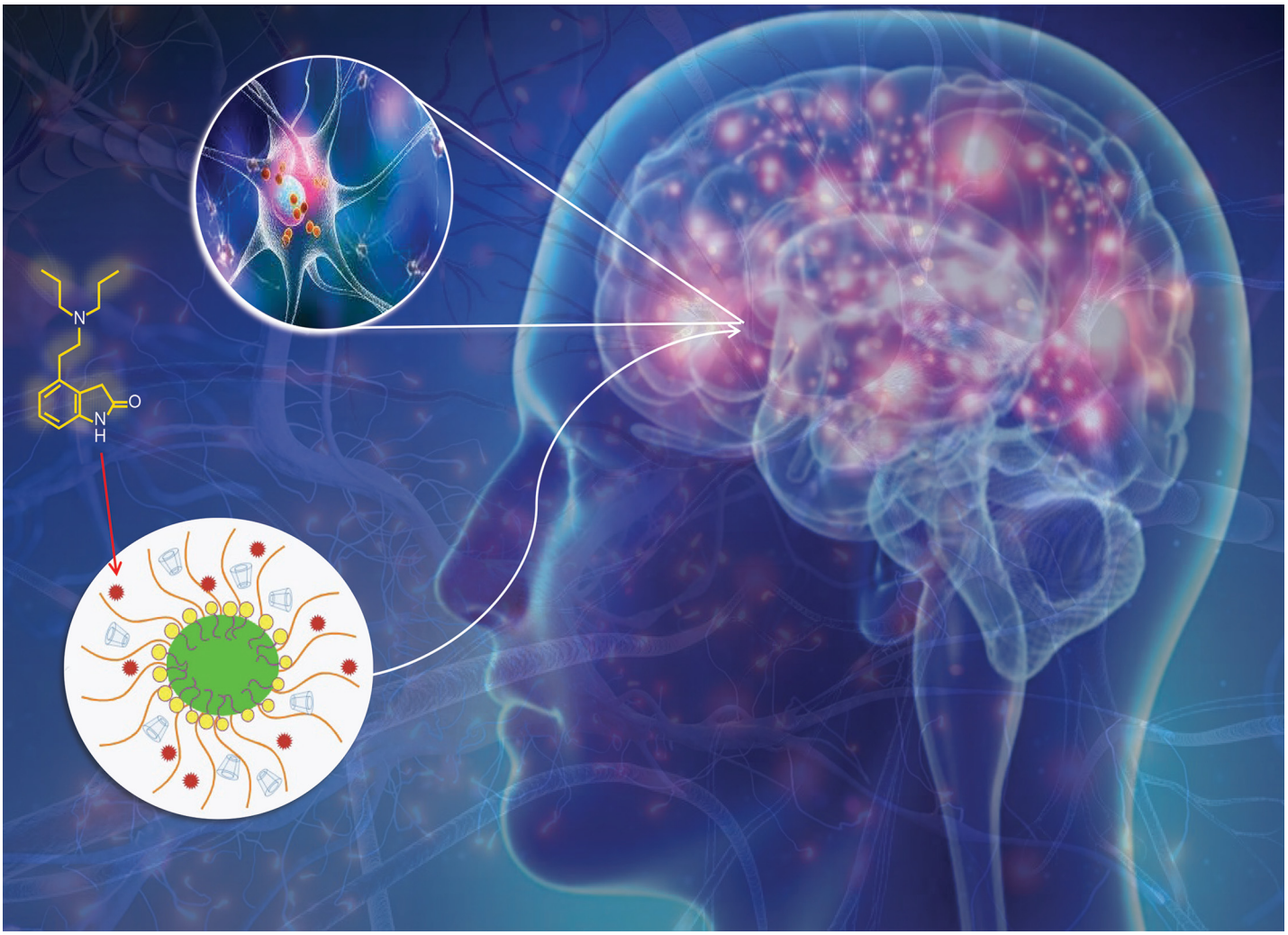

Inspired by nature, this cover showcases innovative hybrid nanoparticles for advanced drug delivery, combining unique biomimetic materials with promising nasal release properties developed at National and Kapodistrian University of Athens and the National Hellenic Research Foundation, Greece.

PEO-*b*-PCL/Tween 80/cyclodextrin systems: from bioinspired fabrication to possible nasal administration of ropinirole hydrochloride

Innovative biomimetic drug delivery systems using poly(ethylene-oxide)-*b*-poly(ε-caprolactone) block copolymers of varying molecular weights and compositions, non-ionic surfactants, and cyclodextrins were self-assembled into hybrid structures with ideal properties for nasal administration of antiparkinsonian drugs.

As featured in:

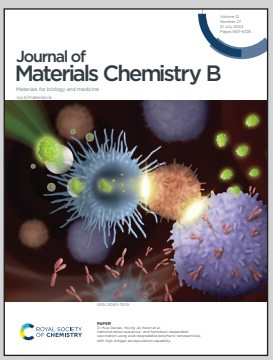

See Natassa Pippa, Stergios Pispas *et al.*, *J. Mater. Chem. B*, 2024, **12**, 6587.

ROYAL SOCIETY OF CHEMISTRY

rsc.li/materials-b

Registered charity number: 207890

Journal of Materials Chemistry B

ROYAL SOCIETY OF CHEMISTRY

PAPER

View Article Online
View Journal | View Issue

Cite this: J. Mater. Chem. B, 2024, 12, 6587

PEO-*b*-PCL/Tween 80/cyclodextrin systems: from bioinspired fabrication to possible nasal administration of ropinirole hydrochloride†

Elmina-Marina Saitani,[a] Natassa Pippa,*[a] Diego Romano Perinelli,[b] Aleksander Forys,[c] Paraskevi Papakyriakopoulou,[a] Nefeli Lagopati,[de] Giulia Bonacucina,[b] Barbara Trzebicka,[c] Maria Gazouli,[d] Stergios Pispas*[f] and Georgia Valsami[a]

In this study, we designed and developed systems composed of poly(ethylene-oxide)-*b*-poly(ε-caprolactone) block copolymers of different molecular weights and compositions, non-ionic surfactant, and cyclodextrins. The innovation of this study lies in the combination of these diverse biomaterials to create biomimetic and bioinspired drug delivery supramolecular structures. The systems were formed by the thin-film hydration method. Extensive physicochemical and morphological characterization was conducted using differential scanning calorimetry, light scattering techniques, microcalorimetry analysis, high-resolution ultrasound spectroscopy, surface tension measurements, fluorescence spectroscopy, cryogenic transmission electron microscopy images, and *in vitro* cytotoxicity evaluation. These innovative hybrid nanoparticles were found to be attractive candidates as drug delivery systems with unique properties by encompassing the physicochemical and thermotropic properties of both classes of materials. Subsequently, Ropinirole hydrochloride was used as a model drug for the purpose of this study. These systems showed a high RH content (%), and *in vitro* diffusion experiments revealed that more than 90% of the loading dose was released under pH and temperature conditions that simulate the conditions of the nasal cavity. Promising drug release performance was observed with all tested formulations, worth further investigation to explore both *ex vivo* permeation through the nasal mucosa and *in vivo* performance in an experimental animal model.

Received 7th March 2024,
Accepted 21st May 2024

DOI: 10.1039/d4tb00489b

rsc.li/materials-b

1. Introduction

Polymers are multifunctional excipients widely used in pharmaceutical technology, with unique properties in drug delivery and targeting.[1] The selection of the most appropriate polymer for creating a novel drug delivery platform is associated with the method of administration, the physicochemical profile of the incorporated drug, the properties of the polymers utilized, the interactions between the different materials of the composite platforms, as well as several other factors.[2]

Research over the past years has led to the identification of amphiphilic block copolymers as potent therapeutic moieties for curing challenging human diseases, which tend to self-assemble in aqueous media, leading to a plethora of nanoassemblies.[3] Poly(ethylene-oxide)-*b*-poly(ε-caprolactone) (PEO-*b*-PCL) block copolymers have attracted the interest of many scientists due to their superior biocompatibility, controlled biodegradability in acidic pH, low toxicity and immunogenicity, simultaneous lipophilic and hydrophilic properties, high loading capacity,[4] as well as targeted and prolonged drug delivery.[5] Concerning the

[a] Department of Pharmacy, School of Health Sciences, National and Kapodistrian University of Athens, Panepistimiopolis, 15771 Zografou, Greece. E-mail: elminasait@pharm.uoa.gr, natpippa@pharm.uoa.gr, ppapakyr@pharm.uoa.gr, valsami@pharm.uoa.gr
[b] School of Pharmacy, Chemistry Interdisciplinary Project (CHIP), University of Camerino, Via Madonna delle Carceri, 62032 Camerino, Italy. E-mail: diego.perinelli@unicam.it, giulia.bonacucina@unicam.it
[c] Centre of Polymer and Carbon Materials, Polish Academy of Sciences, 34, M. Curie-Sklodowskiej St, 41-819 Zabrze, Poland. E-mail: aforys@cmpw-pan.pl, barbara.trzebicka@cmpw-pan.edu.pl
[d] Department of Basic Medical Science, Laboratory of Biology, School of Medicine National and Kapodistrian University of Athens, 11527 Athens, Greece. E-mail: nlagopati@med.uoa.gr, mgazouli@med.uoa.gr
[e] Biomedical Research Foundation, Academy of Athens, 11527 Athens, Greece
[f] Theoretical and Physical Chemistry Institute, National Hellenic Research Foundation, 48 Vassileos Constantinou Avenue, 11635 Athens, Greece. E-mail: pispas@eie.gr

† Electronic supplementary information (ESI) available. See DOI: https://doi.org/10.1039/d4tb00489b

components of PEO-*b*-PCL block copolymers, poly-ε-caprolactone (PCL) is a hydrophobic polymer with a biocompatible and biodegradable nature, having a semi-crystalline bulk structure[6] and low glass transition temperature, composed of repeating units containing an ester group and five methylene groups,[7] whereas polyethylene oxide (PEO) is a biocompatible hydrophilic polymer that provides the system with water solubility and its stealth properties, making it capable of evading the reticuloendothelial system.[5] The literature has already documented the versatile capabilities of PEO–PCL copolymers as nanocarriers.[8] Their stealth properties due to the hydrophilic PEO chain[8] and the chemical versatility of the hydrophobic PCL chain[9] make them capable of facilitating passive and active drug delivery, triggered drug release mechanisms, theranostic applications, and targeted delivery of nucleic acids to specific cells.[8] The properties of the copolymer utilized in each case depend largely on the specific molecular weight and composition.

Cyclodextrins (CDs), also known as cycloamyloses due to their sugar-based backbone, are cyclic oligosaccharides. They consist of six (αCD), seven (βCD), or eight (γCD) D(+)-glucopyranose units linked by α-1,4 glycosidic bonds,[10] creating molecular structures resembling truncated cones.[11,12] Due to their configuration, which is comprised of lipophilic cavities and hydrophilic outer surfaces,[13] they are capable of accommodating a wide range of molecules within their core, resulting in the formation of inclusion complexes through noncovalent interactions.[14] A large gamut of interactions between guests and host molecules contribute to the formation of complexes, like hydrophobic interactions, hydrogen bonds, van der Waals forces, and side effects.

The characteristics of βCD, such as the ideal size of its cavity for the incorporation of molecular agents, easy way of production, low cost, increased drug bioavailability, and improvement of the Active Pharmaceutical Ingredients (APIs) toxicological profile, make it a material of paramount importance for biomedical applications.[15] To ameliorate the low solubility of βCD in water, derivatives of this natural CD with superior characteristics have been developed. In this study, two different derivatives of βCD, methyl-β-CD (MβCD) and hydroxy-propyl-β-CD (HPβCD), were used.

The combination of block copolymers with CDs results in a new class of drug delivery platforms with special properties,[16] *i.e.*, biocompatibility,[17,18] increased loading efficiencies,[19,20] sustained or controlled release properties,[18,21] colloidal stability,[22] a high degree of permeability to biological barriers[17] and targeting to specific cells or tissues.[17]

Considering all these properties, in the present work, we thought it was worthy of investigating the combination of biocompatible block copolymers PEO-*b*-PCL with CDs, namely MβCD and HPβCD, to design and develop complex co-assembled structures that represent a new class of advanced drug delivery systems. More specifically, we designed and developed PEO-*b*-PCL block copolymer/Tw80/MβCD or HPβCD hybrid systems. This combination can result in new biomaterials and supramolecular nanostructures with diverse overall and intrinsic morphology, which inherit the physicochemical and thermotropic properties of all classes of synthetic materials and can be employed for biomimetic drug delivery applications as they can mimic the structure or function of a complex biological system. We also investigated the impact of different compositions of PEO-*b*-PCL block copolymers on the physicochemical, morphological, drug loading, and release characteristics of the prepared hybrid systems. To the best of the authors' knowledge, this is the first time that preformulation, formulation, and characterization studies were performed to investigate the supramolecular co-assembly and interactions in the solid and dispersion states of the selected nanomaterials, especially of block copolymers with an increased ratio of the hydrophobic PCL chain paired with Tw80 and CDs, and of the obtained complex hybrid nanosystems, respectively.

Ropinirole hydrochloride (RH) was used as a drug model for the execution of this study. It is categorized as a non-ergoline dopamine agonist, administered as a monotherapy or in combination with levodopa for the management of Parkinson's disease.[23] It belongs to a biopharmaceutical classification system (BCS) class III drug, presenting high solubility and low permeability while also undergoing extensive first-pass hepatic metabolism. Additionally, it exhibits a short plasma elimination half-life of less than six hours and achieves its maximum plasma concentration in less than one hour.[23] To improve its therapeutic efficacy in clinical practice, alternative routes and drug delivery platforms need to be explored.

In the literature, it has already been reported the combination of PEO-*b*-PCL diblock copolymers with other materials, such as Tw80, Span 80, and cholesterol[2] or dipalmitoylphosphatidylcholine.[24] The innovation of this study is the fact that this is the first report presented in the literature in which the preparation and extensive characterization of systems composed of the combination of these three components (block copolymers, surfactant, and CDs) are prepared and studied for the possible nasal administration of RH.

2. Materials and methods

2.1. Materials

PEO-*b*-PCL amphiphilic diblock copolymers were synthesized *via* ring-opening polymerization of the ε-caprolactone monomer using monohydroxy-PEG as a macroinitiator.[24–26] PEO-*b*-PCL_1, PEO-*b*-PCL_2, and PEO-*b*-PCL_3 block copolymers were produced, containing 15%, 30%, and 53% wt of PCL (hydrophobic component), respectively. The synthetic procedure and the molecular characteristics of the PEO-*b*-PCL block copolymers are described in the ESI† (Table S1). Surfactant Polysorbate 80 (Tween 80 – Tw80), MβCD and HPβCD were purchased from Sigma-Aldrich Chemical Co. (St. Louis, MO, USA) and used without further purification. All formulations were prepared in HPLC-grade water (Fischer Scientific, Pittsburgh, PA, USA). RH was kindly donated by Uni-Pharma S.A. (Athens, Greece). Chloroform, pyrene, and other reagents used were of analytical grade and purchased from Fischer Scientific (Pittsburgh, PA, USA). Pyrene was dissolved in the appropriate concentration (1 mM) in

acetone. The molecular characteristics of the utilized components are presented in Table S2 (ESI†).

2.2. Methods

2.2.1. Differential scanning calorimetry (DSC). Differential scanning calorimetry (DSC) is generally used to obtain information about the physical and energy-exchanging properties of a compound or formulation. DSC experiments were carried out to identify the intramolecular interactions between copolymers, surfactant, and CDs in the solid state, applying the protocol described by Leonis *et al.*[27] In brief, an 822^e Mettler-Toledo (Schwerzenbach, Switzerland) calorimeter was employed and calibrated with pure indium (T_m = 157 °C). Sealed aluminum 40-μL crucibles were used as sample holders. Solid samples of pristine compounds (copolymers, Tw80, MβCD, and HPβCD) and their combinations [Tw80/MβCD at ratio 70 : 30, Tw80/HPβCD at ratio 70 : 30, polymer/Tw80 at ratio 70 : 30, polymer/MβCD at ratio 80 : 20, polymer/HPβCD at ratio 80 : 20, (polymer/Tw80)/MβCD and (polymer/Tw80)/HPβCD at ratio 80 : 20] were investigated. For the analysis, a quantity of 2.0–6.0 mg of dry powder from each sample was placed in the crucible, and afterwards, the crucible was sealed. Before each experiment, the samples were subjected to a constant temperature of 10 °C to ensure equilibration. Each analysis included a heating process in which the sample temperature was changed from 10 °C to 300 °C with a heating rate of 10 °C min^{-1} using a steady flow of nitrogen to provide an inert atmosphere during the measurement to prevent oxidation reactions, while an empty aluminum crucible was used as a reference. The calorimetric data obtained (enthalpy changes $\Delta H_{m/s}$, characteristic transition temperatures $T_{onset,m/s}$ and $T_{m/s}$, and widths at the half peak height of the C_p profiles $\Delta T_{1/2,m/s}$) were analyzed using Mettler-Toledo STAR^e software (version 9.20). For this purpose, the *R*-squared values were assessed.

2.2.2. Preparation of the hybrid systems. The preparation of colloidal dispersions took place by the conventional thin film hydration method. These colloidal dispersions were the systems of pure polymers, polymer/Tw80 systems, polymer/Tw80/MβCD, and polymer/Tw80/HPβCD systems. First, the appropriate amount of each polymer was added to a dry round-bottom flask and dissolved in the minimum volume of chloroform. The organic solvent was removed by rotary evaporation (Hei-VAP series CORE-heidolph®, Schwabach, Germany) under vacuum at 40 °C, and subsequently, a thin film was formed inside the flask wall. Afterwards, the appropriate amount of HPLC-grade water was added to achieve a concentration of colloidal dispersion equal to 10 mg mL^{-1}. The film was hydrated for 30 minutes by slow rotation of the flask in a water bath at 40 °C. Fig. 1 illustrates the chemical structures of the components and the process of the systems' preparation by the thin film hydration method.

To improve the size of the particles formed, probe sonication took place twice for 3 minutes at 70% power, with a 3-minute break between (Bandelin sonopuls, homogenizer, HD3200, Berlin, Germany). Binary polymer/Tw80 and ternary polymer/Tw80/CD systems were also prepared by the procedure

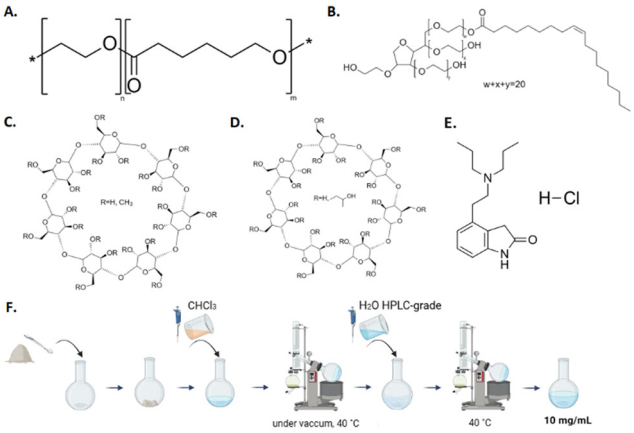

Fig. 1 Chemical structures of the (A) PEO-*b*-PCL block copolymer, (B) Tween 80, (C) methyl-β-cyclodextrin, (D) hydroxypropyl-β-cyclodextrin, (E) ropinirole hydrochloride, and (F) illustration of the systems' preparation by the thin film hydration method.

described above in a molar ratio of 70 : 30 w/w and 80 : 20 w/w, respectively.

2.2.3. Physicochemical characterization of hybrid systems. Particle size, referred to as the average hydrodynamic radius (R_h), polydispersity index (PDI), and zeta potential (z-potential) of the obtained colloidal dispersions were investigated by dynamic and electrophoretic light scattering (DLS and ELS, respectively) using a wide-angle light scattering photometer by ALV GmbH, CGS-3. This setup consists of a He–Ne 22 mW laser source, a compact goniometer system with an Avalanche photodiode detector interfaced with an ALV/LSE-5003 electronics unit, and an ALV-5000/EPP multi-tau digital photon correlator. The Contin method was employed to analyze the results. PDI was determined as a measure of particles' size distribution. Measurements were performed at a scattering angle of 90°, a temperature of 25 °C, and a laser wavelength of 633 nm. 100 μL of each dispersion (10 mg mL^{-1}) were diluted 30 times with HPLC-grade water. Mean values and standard deviations (SD) were calculated from measurements that were repeated three times.

After the preparation, colloidal dispersions were stored in amber glass vials in a refrigerator (4 °C). A physical stability study involved the measurement of a quantifiable physical property, such as particle size *vs.* time from preparation. Measurements of physicochemical characteristics were performed immediately after preparation (T = 0 days), as well as at selected times over a 28-day period, under the above storage conditions.

2.2.4. Biological stability. The alterations in systems' particle size in the conditions that simulate the physicochemical properties of human plasma and nasal cavity were also tested. To achieve this, two different dispersion media were employed: a mixture of Fetal Bovine Serum (FBS) and Phosphate Buffer Solution (PBS) in a ratio of 10 : 90 for simulating human plasma, and a buffer solution with a pH of 5.6 as the dispersion medium to mimic the nasal cavity environment, maintained at a temperature of 34 °C. DLS experiments were conducted for this purpose, as described in Section 2.2.3.

2.2.5. Fluorescence spectroscopy. Fluorescence spectroscopy has been utilized to gain some qualitative information on the internal structure and micro-environment of the prepared systems in HPLC-grade water. Pyrene was used as the hydrophobic probe, able to incorporate itself into the hydrophobic domains of the hybrid platforms. For this reason, the incorporated pyrene was used as a detector of the changes taking place in the internal structure of the colloidal particles. For fluorescence spectroscopy measurements, an appropriate amount of pyrene stock solution was added to each system. The pyrene emission spectra were recorded by a NanoLog Fluorometer (Horiba Jobin Yvon, Piscataway, NJ, USA), using a laser diode as the excitation source (Nano LED, 440 nm, 100 ps pulse width) and a UV TBX-PMT series detector (250–850 nm) from Horiba Jobin Yvon. The method used is described below.

Colloidal dispersions of polymer, polymer/Tw80, polymer/Tw80/MβCD, and polymer/Tw80/HPβCD were prepared at concentrations of 10 mg mL^{-1}, and the appropriate amount (3 μL) of pyrene stock solution (1 mM) was added. The solutions were equilibrated for 24 hours, and then the I_1/I_3 ratio of the first to the third vibronic peak intensities in the pyrene emission spectrum was measured at each hybrid system concentration at a constant temperature of 25 °C. The excitation wavelength for the measurements was 335 nm, and the fluorescence spectra were collected in the range of 355–630 nm. No excimer formation was observed for the solutions examined.

2.2.6. Microcalorimetry (mDSC). Calorimetric analyses were performed using a microDSC III (Setaram, Lyon, France). The prepared colloidal dispersions (Section 2.2.2) were equilibrated for 20 min at a temperature of 5 °C. Then, a heating ramp from 5 °C to 80 °C at a 1 °C min^{-1} rate was performed. Using the software of the instrument (Setsoft2000, Setaram), the melting temperature (T_m, °C) and the enthalpy (ΔH, J g^{-1} of solution) from the peak maximum and the area of the transition, respectively, were calculated. All measurements were performed in triplicate.

2.2.7. High-resolution ultrasound spectroscopy (HR-US). The HR-US 102 high-resolution spectrometer (Ultrasonic Scientific, Dublin, Ireland) was used to determine the differential relative ultrasonic velocity for samples as a function of temperature and at a frequency of 5.4 MHz, preliminarily determined by a broad amplitude frequency scan. Around 2 mL of the prepared colloidal dispersions (Section 2.2.2) and reference (water) were filled in the ultrasonic cells and equilibrated at 5 °C for at least 20 min, and then analyzed by following the same thermal program of mDSC analyses (from 5 °C to 80 °C, at 1 °C min^{-1}). The temperature control was achieved by using a HAAKE C25P thermostat (Thermo Electron Corporation, Langensebold, Hessen, Germany). Ultrasonic sound speed is reported as differential values, calculated by subtracting the contribution of the reference from the value recorded in the sample cell. Sample transitions from ultrasound speed were calculated from the first derivative of the signal. All measurements were performed in triplicate.

2.2.8. Surface tension measurements. The tensiometric analyses on the colloidal systems (Section 2.2.2) were carried out at 20 °C using a DCA-100 contact angle tensiometer (First Ten Angstrom, Newark, CA, USA) according to the Du-Noüy ring method. The surface tension measurements were performed according to the protocol described by Perinelli and coworkers.[28] All analyses were performed in triplicate. The data were the mean ± SD of three independent measurements.

2.2.9. Cryogenic transmission electron microscopy measurements. Cryogenic Transmission Electron Microscopy (cryo-TEM) images were obtained using a Tecnai F20 X TWIN microscope (FEI Company, Hillsboro, Oregon, USA) equipped with a field emission gun, operating at an acceleration voltage of 200 kV. Images were recorded on the Gatan Rio 16 CMOS 4k camera (Gatan Inc., Pleasanton, California, USA) and processed with Gatan Microscopy Suite (GMS) software (version 3.31.2360.0, Gatan Inc., Pleasanton, California, USA). Specimen preparation was done by vitrification of the aqueous solutions on grids with holey carbon film (Quantifoil R 2/2; Quantifoil Micro Tools GmbH, Großlöbichau, Germany). Prior to use, the grids were activated for 15 seconds in oxygen plasma using a Femto plasma cleaner (Diener Electronic, Ebhausen, Germany). Cryo-samples were prepared by applying a droplet (3 μL) of the suspension to the grid, blotting with filter paper, and immediately freezing in liquid ethane using a fully automated blotting device, the Vitrobot Mark IV (Thermo Fisher Scientific, Waltham, Massachusetts, USA). After preparation, the vitrified specimens were kept under liquid nitrogen until they were inserted into a cryo-TEM-holder Gatan 626 (Gatan Inc., Pleasanton, USA) and analyzed in the TEM at −178 °C.

2.2.10. *In vitro* cytotoxicity. Following the physicochemical and thermotropic characterization of the novel hybrid systems, their safety and biocompatibility were evaluated by studying their cytotoxicity *in vitro*. Toxicity was tested using the MTT assay to quantify the reduction in viability following cell exposure to prepared systems by applying the protocol described by Kontogiannis *et al.*[29]

2.2.11. RH quantification in the prepared systems. The quantification of the RH in the prepared systems and its determination in the samples from the *in vitro* experiments were conducted using HPLC-PDA on a Shimadzu prominence system (Kyoto, Japan), which was comprised of an LC-20AD Quaternary Gradient Pump with a degasser, a SIL-HT autosampler, and a SPD-M20A photo-diode array detector. Data acquisition and analysis were executed using the LC Solution® software (LabSolutions, version 1.25 SP4, Kyoto, Japan). For the assessment of the analysis, a Thermo C_{18} ODS Hypershil column (100 × 4.6 mm, 5 μm particle size) in conjunction with a C_{18} precolumn (12.5 × 4.6 mm, 5 μm particle size) was used. The mobile phase consisted of a mixture of acetonitrile and potassium dihydrogen phosphate buffer (0.01 M and pH value adjusted to 2.5) in a 60 : 40 v/v ratio, while the flow rate was configured at 0.8 mL min^{-1}. Each injection involved a volume of 30 μL, and the detection wavelength (λ_{max}) was set at 245 nm. The range of calibration curve samples was 0.5 to 10 μg mL^{-1} of RH. LOD and LLOQ values were found to be equal to 0.10 ± 0.04 μg mL^{-1} and 0.31 ± 0.11 μg mL^{-1}, respectively.

2.2.12. *In vitro* diffusion experiments. *In vitro* diffusion experiments were carried out using two different concentrations of RH, equal to 1 mg mL^{-1} and 5 mg mL^{-1}. Regenerated

cellulose membranes with a molecular cut-off of 1000 Da and Franz-type diffusion cells (Crown Glass, Somerville, MA, USA) were utilized. The preparation procedure involved the immersion of membranes in distilled water for 15 minutes, followed by replacing the water and soaking for an additional 30 minutes. The membranes were then placed in a beaker containing PBS with a pH of 7.4, and they were soaked for 15 minutes. Subsequently, the membranes were cut into 1 cm^2 squares to completely cover the diffusion area of the Franz cells. For each Franz cell, the receptor compartment was filled with 5 mL of PBS (pH 7.4), and the membrane was positioned between the receptor and donor compartments. A magnetic stirrer was placed in the receptor, and the two compartments were secured using a metal clamp. The assembled system was allowed to equilibrate at 34 °C for 15 minutes, mimicking the temperature of the nasal cavity. All formulations were tested using the same dose of RH, which was equal to 0.05 mg. For the formulations containing the RH concentration of 1 mg mL^{-1}, 50 μL of the formulation were introduced into the donor compartment and wet with 50 μL of a buffer solution at pH 5.6. In the case of the other formulation with an RH concentration of 5 mg mL^{-1}, 10 μL of the formulation were placed in the donor compartment and wetted with 90 μL of the buffer solution at pH 5.6. RH solution (0.5 mg mL^{-1}) in buffer with pH 5.6 was also prepared and tested by introducing 100 μL of the solution in the donor compartment.

The experimental duration for all tests was 4 hours. At specific time intervals (15, 30, 45, 60, 90, 120, 150, 180, 210, and 240 minutes), a sample from the receptor compartment was taken and replaced by an equivalent volume of PBS with a pH value equal to 7.4. To quantify the residual amount of RH within the cellulose membrane, a cleansing procedure was performed utilizing a 50 : 50 water/methanol solution. This same protocol was applied to the residual formulation within the donor compartment, facilitating the determination of the remaining RH and subsequent mass balance calculation. The quantification of all samples was achieved by using High-Performance Liquid Chromatography (HPLC), as described in Section 2.2.11.

The diffusion area (A) of the Franz cell is equal to 0.636 cm^2. The flux (J) across the artificial membrane from the donor to the receptor compartment was calculated using the slopes obtained by regression analysis of the amount of RH (Q) permeated per unit area (A) *vs.* time, according to eqn (1).[30]

$$J = \frac{dQ}{dt \times A} \quad (1)$$

2.2.13. Statistical analysis. The experimental data were assessed using the GraphPad Prism 5.0 software package (GraphPad Software, version 5.01). A significance level of $p < 0.05$ was chosen, and all tests were two-tailed with a 95% Confidence Interval (CI). To identify outliers, the interquartile range (IQR) method with a 1.5 × IQR threshold was employed, but no outliers were detected. One-way ANOVA with Bonferroni *post hoc* tests for multiple comparisons was conducted to identify potential statistically significant variations among all the pairs of compared groups. The results are presented as the mean ± SD for the results of *in vitro* cytotoxicity studies and *in vitro* diffusion experiments. Permeation values were subjected to statistical comparisons both among the tested formulations and at each time point within each formulation.

3. Results and discussion

3.1. Preformulation studies – investigation of the thermotropic behavior of hybrid systems

The initial stage in accomplishing the design and development of hybrid systems composed of different materials is to determine the interactions between them. DSC is an appropriate technique for the investigation of these interactions and a useful tool for further formulation studies. The calorimetric heating profiles of pure compounds and the binary mixtures (polymer/Tw80 and polymer/CD) in the solid state obtained by DSC analysis are shown in Fig. S1 and S2, respectively (ESI†). Fig. 2 shows the DSC thermograms for Tw80/CD mixtures and ternary systems in the solid state, and the corresponding calorimetric parameters are summarized in Table S3 (ESI†).

The findings extracted from the DSC experiments for pure compounds of Tw80, MβCD, and HPβCD, as well as their combinations (Tw80/MβCD 70 : 30 and Tw80/HPβCD 70 : 30), are comprehensively documented in our recent study.[31] Briefly, the thermogram analysis of Tw80 (ESI,† Fig. S1B) showed a broad endothermic peak at 60 °C, which may be coincident with the cloud point of Tw80 at 65 °C.[32] The DSC scan for pure MβCD is characterized by one broad endothermic peak at 180 °C and one another at 75 °C with a low value of enthalpy (ESI,† Fig. S2A), whereas DSC analysis for HPβCD revealed an endothermic peak at 147 °C (ESI,† Fig. S2B), which may be associated with the water loss of the crystal as well as the absence of a defined fusion event since they do not present a crystalline structure.[33]

Comparing the two βCD derivatives, it is observed that HPβCD not only presents a lower main transition temperature (T_m = 147 °C) than MβCD (T_m = 180 °C) but also a higher value of enthalpy (ESI,† Table S3), indicating that the MβCD derivative is more resistant to temperature increase and requires more energy to reach its melting point (apparently intermolecular secondary interactions are stronger in this system).

The Tw80/MβCD mixture exhibited significant changes in thermal behavior, as evidenced by DSC analysis. The broad endothermic peak of pure Tw80 was replaced by two peaks in the mixture: one broad exothermic peak at 148 °C and one endothermic peak at 187 °C (Fig. 2A). These results suggest interactions between Tw80 and MβCD, likely involving secondary bonding interactions such as van der Waals forces. The transition temperatures in the mixture were closer to those of MβCD, indicating its substantial influence on the surfactant's behavior. Similarly, the Tw80/HPβCD mixture showed a shift in the endothermic peak of Tw80 to a higher temperature (132 °C), closer to that of pure HPβCD (147 °C), indicating significant interactions between the components (Fig. 2B).

Concerning the thermograms of pure PEO-*b*-PCL polymers, the DSC scan reveals a main intense endothermic peak at

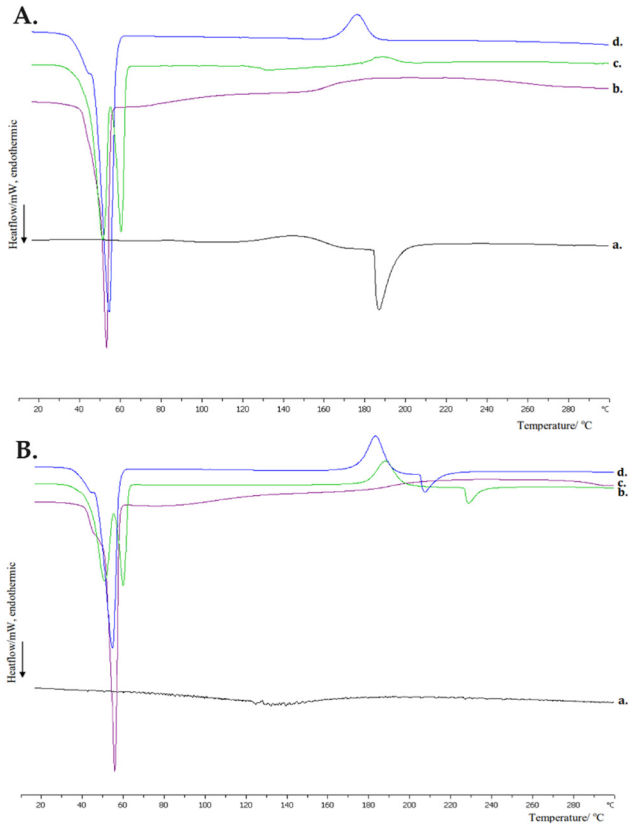

Fig. 2 DSC thermograms. The heating curves of (A) a. Tw80/MβCD, b. PEO-*b*-PCL_1/Tw80/MβCD, c. PEO-*b*-PCL_2/Tw80/MβCD, d. PEO-*b*-PCL_3/Tw80/MβCD, (B) a. Tw80/HPβCD, b. PEO-*b*-PCL_2/Tw80/HPβCD, c. PEO-*b*-PCL_1/Tw80/HPβCD, d. PEO-*b*-PCL_3/Tw80/HPβCD. The limits for the calculation of thermotropic parameters are from 10 °C to 300 °C. The pretransition and main transition phenomena are identified and quantified.

around 58–63 °C (ESI,† Fig. S1A), accompanied by a pretransition peak with a low value of enthalpy at the beginning of the main peak. Additionally, DSC curves of polymers present an exothermic peak at higher temperatures ($T_{PEO\text{-}b\text{-}PCL_1}$ = 195 °C, $T_{PEO\text{-}b\text{-}PCL_2}$ = 194 °C, $T_{PEO\text{-}b\text{-}PCL_3}$ = 187 °C), which have similar values of enthalpy, except for the PEO-*b*-PCL_2 polymer. A very broad exothermic peak with an extremely high value of enthalpy is also apparent in these DSC thermograms.

Concerning the binary polymer/Tw80 systems (ESI,† Fig. S1B), a displacement of the main transition temperature to lower temperatures is observed, ranging from 2 °C to 10 °C, with the highest reduction observed in the PEO-*b*-PCL_2/Tw80 mixture. The peaks are sharper than pure polymer peaks, accompanied by a reduction in enthalpy. In addition to this, in the PEO-*b*-PCL_2/Tw80 system, there is an evident separation of the main and pretransition peaks observed in the pure polymer compound. Low values of $\Delta T_{1/2}$ (half width at half peak height of the transition) (ESI,† Table S3) prove the good cooperativity between the compounds, which is a result of the stabilization of the mixed systems. The viscous liquid nature of the Tw80 could also be responsible for this result.[34]

The DSC curves of binary systems evidence thermal interactions between polymers and surfactant, as indicated by the disappearance of all exothermic peaks. The driving force for these changes in thermal behavior is the amphiphilicity of the materials. Both compounds in the binary systems have an amphiphilic character, which permits them to interact with each other not only with hydrophilic interactions but also with hydrophobic ones. More specifically, the hydrophilic chains of PEO-*b*-PCL block copolymers (*i.e.*, PEO chains) interact with the head group of Tw80 and the hydrophobic PCL chains of polymers with the hydrophobic subunits of surfactant, respectively. The formation of hydrogen bonds and/or van der Waals interactions may be attributed to these alterations.

DSC curves of polymer/MβCD mixtures (ESI,† Fig. S2A) show translocation of the endothermic peaks to lower temperatures, with the highest reduction observed in the PEO-*b*-PCL_2/MβCD mixture, thus resulting in the hypothesis that the hydrophobic PCL chains of polymers interact with the lipophilic cavity of MβCD *via* van der Waals interactions and simultaneously the hydrophilic PEO chains interact with the outer hydrophilic part of MβCD. We could note that the cooperativity of the polymers with MβCD is better in comparison with those observed for polymer/Tw80 systems, as the peaks are sharper and $\Delta T_{1/2}$ values are diminished (ESI,† Table S3). Enthalpy is reduced in all hybrid systems, except for the PEO-*b*-PCL_1/MβCD mixture, in which it presents a slight increase (ESI,† Table S3).

The incorporation of MβCD does not have a notable impact on the transition temperature of polymer exothermic peaks, but a considerable reduction of the PEO-*b*-PCL_2/MβCD mixture enthalpy is observed. Moreover, a new endothermic peak appeared in the PEO-*b*-PCL_3/MβCD mixture at 272 °C (ESI,† Fig. S2A), indicating a possible complex formation or at least an interaction between PEO-*b*-PCL_3 block copolymer and MβCD in the solid state.

Alternatively, this high temperature may be indicative of some sort of mixture's decomposition. In the literature,[26,27] it has been reported that CDs decompose above 300 °C. Therefore, the discrepancies in our results may be related to the compound purity and mode of sample preparation before measurements.

Compared with pure polymers, the DSC curves of polymer/Tw80/MβCD ternary systems displayed a completely different peak pattern (Fig. 2A). The exothermic fusion peaks of PEO-*b*-PCL compounds disappeared, and new peaks came into sight: exothermic peaks at lower temperatures and endothermic broad peaks at 147 °C and 132 °C for PEO-*b*-PCL_1 and PEO-*b*-PCL_2 hybrid systems, respectively. The last endothermic peak was absent in the ternary system containing the PEO-*b*-PCL_3 polymer.

Additionally, the results indicated a decrease in the main transition temperatures of the sharp endothermic peaks appearing in the DSC curves of pure polymers in the range of 4–11 °C, with the highest reduction observed for the PEO-*b*-PCL_2 ternary system. The values of enthalpy were reduced in the range of 3–10 kJ mol^{-1} (ESI,† Table S3), demonstrating the development of strong interactions and better cooperativity of the components under these conditions. As outlined in previous studies, the reduction in ΔH values associated with a DSC

curve of a specific component after the addition of another material signifies enhanced interactions between the two compounds.[35]

Based on the findings above, it can be inferred that an inclusion complex might be formed between the hydrophobic chains of polymers (PCL chains) and surfactant with the core of MβCD, while the hydrophilic/outer surface of MβCD interacts with the hydrophilic parts of amphiphilic polymers (*i.e.*, PEO chains) and surfactant (ethylene oxide subunits). Hydrogen bonds and van de Waals interactions may contribute to this complexation. Therefore, MβCD can increase the water solubility of the amphiphilic block copolymer/surfactant mixture by forming inclusion complexes through its hydrophobic interior and hydrophilic exterior. The hydrophobic regions of the copolymer and surfactant may be enveloped within the hydrophobic interior of MβCD, aiding the solubilization of the systems. Previous studies have documented the development of inclusion complexes between polymers and CDs through the utilization of DSC analysis. Zhang *et al.* conducted a study wherein they illustrated the formation of an inclusion complex.[36] This was achieved by incorporating hydrophobic polymer groups into the lipophilic cavity of βCD through van der Waals forces and hydrophobic interactions during the complexation process.

Regarding the combination of HPβCD and polymers, there is a slight shift of endothermic peaks at lower temperatures, ranging from 2 °C to 10 °C, whereas at the same time, the transition temperatures of the polymer's exothermic peaks remain more or less unaffected. One interesting observation is that the presence of HPβCD converted the broad exothermic peak of the PEO-*b*-PCL_2 polymer to a sharper, more symmetric peak with low associated enthalpy. Also, one significant notice is the disappearance of the PEO-*b*-PCL_3 exothermic peak, as well as the appearance of new endothermic peaks in DSC thermograms of PEO-*b*-PCL_1 and PEO-*b*-PCL_2 block copolymers at around 264 °C, which may be attributed to the possible creation of a more water-soluble complex and the incorporation of polymer chains into the CD's core or the possible decomposition of the polymer/HPβCD mixture.

Concerning the cooperativity of the materials, HPβCD/polymer mixtures present sharper [decreased values of $\Delta T_{1/2}$ (ESI,† Table S3)] and more symmetric DSC peaks (ESI,† Fig. S1D) compared to polymer/MβCD mixtures. This result may be attributed to the different hydrophobicity of βCD derivatives since MβCD is a methylated form of βCD and HPβCD is obtained by the incorporation of a hydroxyl propyl group into βCD upon reaction with propylene oxide.[37] These changes at βCD substitution permit the development of different interactions between the compounds and consequently the appearance of different thermal behaviors.

According to the results of DSC experiments for ternary polymer/Tw80/HPβCD systems (Fig. 2B), the incorporation of HPβCD into binary polymer/Tw80 systems influenced each polymer's behavior in a completely different way. Regarding the PEO-*b*-PCL_1/Tw80 system, the main transition peak appears almost unaffected, whereas the presence of a new endothermic peak with a very low value of enthalpy is observed at 181 °C. The impact of HPβCD on the PEO-*b*-PCL_2/Tw80 system is obvious due to the appearance of two new peaks: one exothermic at 188 °C and one endothermic at 229 °C. Lastly, DSC curves of ternary systems containing PEO-*b*-PCL_3 revealed the same pattern of influence in the PEO-*b*-PCL_2/Tw80 system, with the existence of a new endothermic peak at 208 °C and an exothermic peak at 183 °C. We should also point out that the cooperativity of the materials in the ternary polymer/Tw80/HPβCD systems is greater than the majority of systems with MβCD, as evidenced by the lower values of $\Delta T_{1/2}$ (ESI,† Table S3). Finally, the obtained data let us conclude that an inclusion complex may have been created in this mixture.

To sum up, DSC analysis demonstrated the existence of a repertoire of interactions between the compounds. Non-ionic surfactant Tw80 interacted with polymers, affecting their

Table 1 Physicochemical characteristics and I_1/I_3 values of colloidal dispersions at the temperature of 25 °C

Colloidal dispersions	w/w	Number of peaks	$R_{h\ (Contin)}$[a] (nm)	Weight of peak (%)	PDI[b]	z-potential (mV)	I_1/I_3
PEO-*b*-PCL_1	—	1	172	100	0.7_9	−9.2 ± 5.0	1.33
PEO-*b*-PCL_2	—	1	35	100	0.2_1	−11.6 ± 0.5	1.39
PEO-*b*-PCL_3	—	1	41	100	0.7_5	−6.3 ± 6.3	1.36
PEO-*b*-PCL_1/Tw80	70 : 30	1	147	100	0.9_7	−7.0 ± 6.5	1.23
PEO-*b*-PCL_2/Tw80	70 : 30	1	26	100	0.32	−8.6 ± 5.0	1.30
PEO-*b*-PCL_3/Tw80	70 : 30	1	64	100	0.7_6	−9.6 ± 3.0	1.30
(PEO-*b*-PCL_1/Tw80)/MβCD	80 : 20	2	(1) 12 (2) 116	(1) 7 (2) 93	0.3_6	−10.9 ± 7.6	1.26
(PEO-*b*-PCL_2/Tw80)/MβCD	80 : 20	2	(1) 13 (2) 120	(1) 14 (2) 85	0.4_7	−14.7 ± 1.0	1.25
(PEO-*b*-PCL_3/Tw80)/MβCD	80 : 20	2	(1) 19 (2) 96	(1) 38 (2) 62	0.4_3	−1.3 ± 1.1	1.29
(PEO-*b*-PCL_1/Tw80)/HPβCD	80 : 20	2	(1) 10 (2) 99	(1) 5 (2) 95	0.3_6	−1.9 ± 3.7	1.26
(PEO-*b*-PCL_2/Tw80)/HPβCD	80 : 20	2	(1) 12 (2) 120	(1) 15 (2) 85	0.5_1	−21.0 ± 11.5	1.26
(PEO-*b*-PCL_3/Tw80)/HPβCD	80 : 20	2	(1) 17 (2) 88	(1) 40 (2) 60	0.4_7	−8.6 ± 10.6	1.25

[a] R_h indicates the average hydrodynamic radius of three replicates of each sample measured by the Contin method. [b] PDI indicates the average polydispersity index.

thermotropic behavior, whereas the further incorporation of βCD derivatives significantly changed the thermal profile of the compounds due to the possible creation of an inclusion complex.

3.2. Physicochemical characterization of systems in aqueous solutions

Table 1 presents the particle size, expressed as R_h, the weight of peak (% with respect to scattered light intensity), and the PDI of the prepared colloidal dispersions on the day of their preparation (day 0), as well as their z-potential values. The z-potential serves as a significant parameter, offering insights into the surface charge of the suspended colloidal particles. It is imperative to note that the particle preparation protocol and composition crucially influence the above parameters.

By analyzing the DLS results, there was a variety in the average particle size of the systems on day 0 based on their different compositions. PDI also varies significantly between the systems, and it reflects the heterogeneity of particle size distribution. The small value of PDI, close to zero, indicates monodisperse systems with a narrow size distribution, whereas a large one, close to one, indicates largely heterogeneous systems. Concerning the obtained results, we can point out that the composition of the systems and consequently the content of the hydrophobic component is a parameter that significantly influences the size of the resulting particles. Indeed, the colloidal dispersions of copolymers with a higher content of PCL (PEO-*b*-PCL_2 and PEO-*b*-PCL_3) presented lower values of R_h in comparison with PEO-*b*-PCL_1. Namely, PEO-*b*-PCL_2 and PEO-*b*-PCL_3 exhibited R_h around 35 nm and 41 nm respectively, whereas for PEO-*b*-PCL_1 R_h was equal to 172 nm.

Furthermore, it is well known in the literature that not only the composition but also the molar mass of the copolymer, MW, has a crucial impact on the size and polydispersity of the studied particles.[4] Regarding their size polydispersity, the PEO-*b*-PCL_2 system presented a lower PDI value (0.2_1) and consequently better particles' heterogenicity as opposed to PEO-*b*-PCL_1 and PEO-*b*-PCL_3. PDI values for these systems were around 0.7–0.8, and they presented different particle populations. Thus, it is evident that the reduction in MW affects proportionally the formation of smaller and more uniform particles in the colloidal dispersions containing only the pure polymers.

Regarding the polymer/Tw80 binary systems, the addition of Tw80 influenced each polymer in a different way. On the one hand, the particle size of the PEO-*b*-PCL_3/Tw80 system appeared to be around 64 nm, presenting an increase in particle size in comparison to the corresponding system of pure polymer. Nevertheless, this mixture presented a high polydisperse population, as proven by the high value of PDI (Table 1).

On the other hand, PEO-*b*-PCL_1/Tw80 and PEO-*b*-PCL_2/Tw80 presented lower R_h values, 147 nm and 26 nm respectively, compared to systems without the presence of surfactant. The PEO-*b*-PCL_2/Tw80 system was comprised of a more uniform particle population compared with the other binary systems (Table 1).

These observed changes in particle size are in line with the results obtained by DSC experiments. Indeed, the evidenced alterations in the DSC curves of the systems proved the existence of interactions and co-assembly phenomena between the compounds, leading to modifications in the particle size of the systems in aqueous solutions.

Additionally, it is worth noting that the presence of different βCD derivatives led to significant alterations between the prepared colloidal dispersions. In all cases, the incorporation of CD resulted in the emergence of two distinct particle populations: a smaller one (R_h equal to 10–19 nm) and a bigger one (R_h equal to 88–120 nm). Notably, the population with the highest R_h was the most dominant one in all cases. It is worth noting that the PEO-*b*-PCL_1 and PEO-*b*-PCL_3 displayed higher homogeneity, as evidenced by lower PDI values, in comparison to the corresponding pure polymer and polymer/Tw80 binary systems. Conversely, the addition of CDs in PEO-*b*-PCL_2 systems had the opposite effect on system uniformity, resulting in higher PDI values (Table 1). It is noteworthy that the observed differences in particle sizes among ternary systems were not significantly distinct. It may indicate that after the addition of the CD derivative, the contribution of the hydrophobic component (different wt% of PCL) may not be pivotal, whereas hydrophilic interactions between the compounds seem to prevail.

ELS measurements of the prepared structures in an aqueous medium revealed a slightly negative surface potential. It should be highlighted that for the majority of the composed systems, z-potential was found to be around zero, except for PEO-*b*-PCL_2/Tw80/MβCD and PEO-*b*-PCL_2/Tw80/HPβCD ternary systems, which presented a higher negative z-potential value, corresponding to the values of −14.7 and −21.0 mV, respectively (Table 1). Values of z-potential around zero mean an absence of charges around the particle surfaces. Furthermore, the different composition of polymers (content of the hydrophobic part), as well as the presence of both surfactant and βCD derivatives did not affect the surface charge (no electrostatic repulsion between the particles seems to exist) (Table 1).

3.3. Physical and biological stability studies

The physicochemical stability of the ternary systems throughout a period of 28 days was also examined. For this purpose, the final dispersions were placed in a glass vial and stored in the refrigerator at 4 °C, and DLS measurements were repeated over a one-month systematic measurement period.

Fig. S3 (ESI†) illustrates the stability assessment of ternary systems through R_h measurements during the 28-day period. The results proved that PEO-*b*-PCL_1/Tw80/MβCD, PEO-*b*-PCL_1/Tw80/HPβCD, PEO-*b*-PCL_2/Tw80/MβCD, PEO-*b*-PCL_2/Tw80/HPβCD, and PEO-*b*-PCL_3/Tw80/HPβCD systems remained stable during this period as their R_h did not change significantly. However, it is worth noting that on the last day of the stability study, a slight increase in R_h of approximately 30–40 nm was observed in the dominant population of the PEO-*b*-PCL_2/Tw80/HPβCD and PEO-*b*-PCL_3/Tw80/HPβCD systems.

This may be attributed to possible aggregation phenomena, as evidenced by the broadened curves in the size distribution diagram (ESI,† Fig. S3D and F). The PEO-*b*-PCL_3/Tw80/MβCD system exhibited physical instability during the stability studies, as evidenced by variations in the R_h of its particle population between measurements. Initially, two populations with R_h values of 19 nm and 96 nm were observed on the first day of preparation. However, on the 7th day of the stability study, these two populations were replaced by three new populations with different R_h values. Furthermore, the resultant particles showed a significant increase in R_h values at the last measurement, indicating possible aggregation of the particles (ESI,† Fig. S3E).

Overall, most systems exhibited z-potential values close to 0, indicating a lack of significant electrostatic interactions. However, excluding PEO-*b*-PCL_3/Tw80/MβCD, all systems remained stable throughout the entire stability study period. Hence, the observed physical stability cannot be attributed to electrostatic interactions between particles. In our opinion, the steric repulsion between the hydrophilic polymeric blocks is responsible for the long-term stability of the dispersions, which is a property provided by the hydrophilic corona of the PEO chains of each polymer. In conclusion, the presented experiments give valuable guidelines for the preparation of complex, mixed colloidal amphiphilic systems suitable for pharmaceutical formulations.

The FBS/PBS (10 : 90) mixture was utilized as a dispersion medium to mimic the physicochemical conditions of the blood (ESI,† Table S4, Fig. S4). In all cases, there was a rise in the particle size of ternary systems, accompanied by the appearance of new populations. Notably, the dominant population in the PEO-*b*-PCL_2/Tw80/MβCD system exhibited the highest rise in R_h, reaching an increase of 72 nm. The broadening of the size distribution curves in the systems, as depicted in Fig. S4 (ESI†), indicates a significant level of heterogenicity within the population. This high polydispersity is likely caused by aggregation phenomena induced by the plasma proteins.

The experimental results presented above suggest that the hybrid systems possess stealth characteristics to a certain extent, as evidenced by the main populations falling within the range observed when using water HPLC-grade as the dispersion medium. This can be attributed to the protective function of PEO polymeric chains in the PEO-*b*-PCL block copolymers, which effectively shield the nanostructures from environmental factors and extend their presence in the bloodstream. The stealth characteristics provided by the hydrophilic corona that was formed by the PEO chains of the PEO-*b*-PCL block copolymer have also been documented in previous studies.[38–40]

Furthermore, the ternary systems containing PEO-*b*-PCL_1 and PEO-*b*-PCL_2 block copolymers did not show any significant alterations in size when exposed to conditions that mimic the nasal cavity. Under specific conditions of a pH of 5.6 and a temperature of 34 °C, the systems maintained their initial size without any significant change (ESI,† Table S4 and Fig. S4). These results strongly suggest that these formulations maintain their structural integrity and stability when subjected to simulated nasal cavity conditions, with the PEO chains contributing partially to the biological stability of the composite structures. It should be noted that PEO-*b*-PCL_3/Tw80/MβCD and PEO-*b*-PCL_3/Tw80/HPβCD ternary systems showed an increase in dominant population R_h equal to 23 and 41 nm, respectively. This outcome is reasonable since the percentage of PEO chains is lower compared to the other PEO-*b*-PCL polymers, resulting in a reduced protective effect.

3.4. Fluorescence spectroscopy results

In a similar context, fluorescence spectroscopy measurements were conducted to extract information on the internal structure of the hybrid systems, using pyrene as the hydrophobic probe. It is known that this compound is able to be encapsulated into the hydrophobic domains of amphiphilic polymeric mixed structures formed in aqueous solutions. The ratio of intensities between the first and third peaks appearing in the pyrene emission spectrum, I_1/I_3, is a sensitive measure of the polarity of the environment around the probe. As it is known from the literature,[41] I_1/I_3 ratio values of 1 to 1.3 demonstrate the existence of a hydrophobic microenvironment, while I_1/I_3 ratio values in the range of 1.7 to 1.9 typically represent a polar environment. Fluorescence Spectroscopy analysis was implemented using the same temperature conditions (25 °C) for all the systems prepared, and Table 1 presents the I_1/I_3 values determined for them.

From the presented data, it is evident that the addition of surfactant decreased the ratio I_1/I_3, and consequently, the micropolarity of the hybrid systems decreased due to interactions occurring between the amphiphilic compounds. Moreover, the incorporation of βCD derivatives (MβCD and HPβCD) influenced the behavior of block copolymers in a different way. Despite the fact that it caused an increase in I_1/I_3 values in PEO-*b*-PCL_1/Tw80 systems, it affected the PEO-*b*-PCL_2/Tw80 and PEO-*b*-PCL_3/Tw80 systems in the opposite way, reducing the I_1/I_3 values in comparison to the colloidal dispersions composed of pure polymers. Therefore, it is obvious that the presence of CDs caused a decrease in the hydrophobicity of the system containing the most hydrophilic block copolymer (PEO-*b*-PCL_1) and simultaneously an enhancement to those systems with the most hydrophobic copolymers (PEO-*b*-PCL_2 and PEO-*b*-PCL_3). These results were observed in both MβCD and HPβCD derivatives. These observations indicate a significant influence in hydrophilic interactions among the compounds, presumably facilitated by interactions between the hydrophilic PEO chains of the polymer, the head group of Tw80, and the hydrophilic surface of CDs. Nevertheless, in most cases, the changes observed in I_1/I_3 values are very low.

3.5. Thermal characterization of colloidal dispersions by mDSC and HR-US

Having obtained essential information regarding the physicochemical characteristics of the studied systems, their thermotropic behavior was determined *via* mDSC and HR-US. The derived results from the above techniques are presented in Table 2.

Regarding the systems containing only the polymers, it was noticed that there were not any detectable transitions in the thermograms obtained by the above techniques. The absence of detectable transitions suggests that at the concentration used,

the copolymers did not assemble, or in the range of temperature studied, there was no detectable energetic contribution in the self-assembling process.

A very small transition was found for the binary systems composed of PEO-*b*-PCL block copolymers and surfactant. The appearance of the curves proved the presence of thermal interactions between polymers and surfactant, which were forced by the amphiphilic character of the compounds, permitting them to interact with each other through hydrophilic and hydrophobic interactions. More specifically, PEO-*b*-PCL_1/Tw80, PEO-*b*-PCL_2/Tw80, and PEO-*b*-PCL_3/Tw80 revealed an endothermic peak at 54 °C, 55 °C, 51 °C and ΔH values of 0.012 J g^{-1}, 0.016 J g^{-1}, and 0.010 J g^{-1} respectively (Table 2). The PEO-*b*-PCL_1/Tw80 system presented a sharper endothermic peak compared to the other binary systems (Fig. 3B).

Furthermore, mDSC results revealed that there was no noteworthy dependence on the content of the hydrophobic part on the thermal behavior of PEO-*b*-PCL block copolymers since all copolymer systems were characterized by a very low value of enthalpy, which is almost impossible to detect by mDSC.

The incorporation of MβCD into the systems led to a decrease in the main transition temperature of PEO-*b*-PCL_1/Tw80 and PEO-*b*-PCL_2/Tw80 systems to less than 5 °C, whereas the transition temperature of PEO-*b*-PCL_3/Tw80 remained almost unaffected. ΔH values ranged at the same levels, except for PEO-*b*-PCL_2/Tw80/MβCD, which increased twice as much (Fig. 3C and Table 2). The mDSC results obtained after the incorporation of HPβCD revealed a slight displacement of endothermic peaks at lower temperatures, ranging from 2 °C to 4 °C compared with binary systems ($T_{\text{PEO-}b\text{-PCL}_1\text{/Tw80/HP}\beta\text{CD}}$ = 52 °C, $T_{\text{PEO-}b\text{-PCL}_2\text{/Tw80/HP}\beta\text{CD}}$ = 51 °C, $T_{\text{PEO-}b\text{-PCL}_3\text{/Tw80/HP}\beta\text{CD}}$ = 51 °C). A slight decrease of ΔH values was also observed for PEO-*b*-PCL_2/Tw80/HPβCD (ΔH = 0.012 J g^{-1}), while PEO-*b*-PCL_3/Tw80/HPβCD thermograms showed a minor increase (ΔH = 0.018 J g^{-1}) and PEO-*b*-PCL_1/Tw80/HPβCD ranged in the same levels (ΔH = 0.012 J g^{-1}) (Fig. 3D and Table 2).

The hydrophobic PCL chains of polymers and non-polar parts of Tw80 may be incorporated into the hydrophobic core of CDs. Thus, this three-dimensional configuration of the system in the solution state with the combination of the self-assembly ability of colloidal dispersions could lead to the enhancement

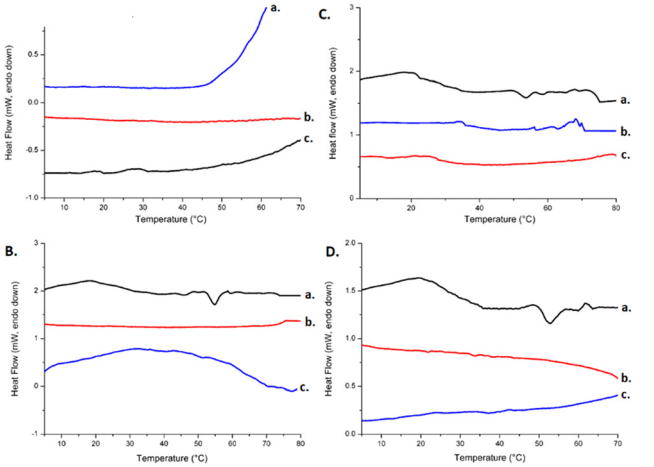

Fig. 3 mDSC traces for (A) a. PEO-*b*-PCL_3, b. PEO-*b*-PCL_2, c. PEO-*b*-PCL_1, (B) a. PEO-*b*-PCL_1/Tw80, b. PEO-*b*-PCL_2/Tw80, c. PEO-*b*-PCL_3/Tw80, (C) a. PEO-*b*-PCL_1/Tw80/MβCD, b. PEO-*b*-PCL_2/Tw80/MβCD, c. PEO-*b*-PCL_3/Tw80/MβCD, and (D) a. PEO-*b*-PCL_1/Tw80/HPβCD, b. PEO-*b*-PCL_2/Tw80/HPβCD, c. PEO-*b*-PCL_3/Tw80/HPβCD.

of the water solubility of the systems and consequently to the absence of intense peaks with high enthalpy values in mDSC thermograms compared to the systems in the solid state.

Observing the mDSC thermograms of ternary systems, we should notice that the mDSC curves of PEO-*b*-PCL_1/Tw80/HPβCD, which contained the PEO-*b*-PCL copolymer with the highest content of polar PEO, exhibited a significantly sharper endothermic peak compared to the corresponding ternary system containing MβCD (Fig. 3C and D). We should point out that the slight differences observed in the thermal behavior of ternary systems with MβCD and HPβCD in solution state may be ascribed to the structures of CDs and consequently to their different water solubility. To confirm the information taken from mDSC, the HR-US technique was also applied (Fig. 4).

The calculation of the transition using the HR-US method is presented as a stepwise deviation of the linearly decreasing sound speed signal over temperature.[42] Transition temperatures can be easily calculated from the first derivate of sound speed *vs.* temperature signals and are reported in Table 2.

Table 2 Thermodynamic parameters (transition temperature, °C, and associated enthalpy, J g^{-1} of solution) and surface parameters of the prepared systems for the prepared formulations as calculated from mDSC, HR-US, and surface tension measurements. The data represent the mean ± SD of three replicates

	mDSC		HR-US (sound speed)	Surface tension measurements
Colloidal dispersion	Temperature (°C)	Enthalpy (J g^{-1})	Temperature (°C)	Surface tension (mN m^{-1})
PEO-*b*-PCL_1/Tw80	54.34 ± 0.76	0.012 ± 0.004	53.44 ± 0.77	46.80 ± 0.55
PEO-*b*-PCL_2/Tw80	55.37 ± 0.89	0.016 ± 0.009	55.28 ± 0.06	51.80 ± 0.57
PEO-*b*-PCL_3/Tw80	50.97 ± 1.01	0.010 ± 0.006	51.27 ± 0.24	53.26 ± 0.45
PEO-*b*-PCL_1/Tw80/MβCD	50.71 ± 0.65	0.011 ± 0.004	52.59 ± 0.67	41.27 ± 0.41
PEO-*b*-PCL_2/Tw80/MβCD	50.46 ± 0.45	0.029 ± 0.009	49.12 ± 0.93	40.32 ± 0.33
PEO-*b*-PCL_3/Tw80/MβCD	51.23 ± 0.48	0.011 ± 0.009	53.12 ± 0.33	41.26 ± 0.48
PEO-*b*-PCL_1/Tw80/HPβCD	52.22 ± 0.75	0.012 ± 0.005	54.13 ± 0.78	39.11 ± 0.97
PEO-*b*-PCL_2/Tw80/HPβCD	51.10 ± 0.74	0.012 ± 0.006	53.26 ± 0.45	37.64 ± 0.18
PEO-*b*-PCL_3/Tw80/HPβCD	51.36 ± 0.89	0.018 ± 0.009	53.08 ± 0.38	43.41 ± 0.45

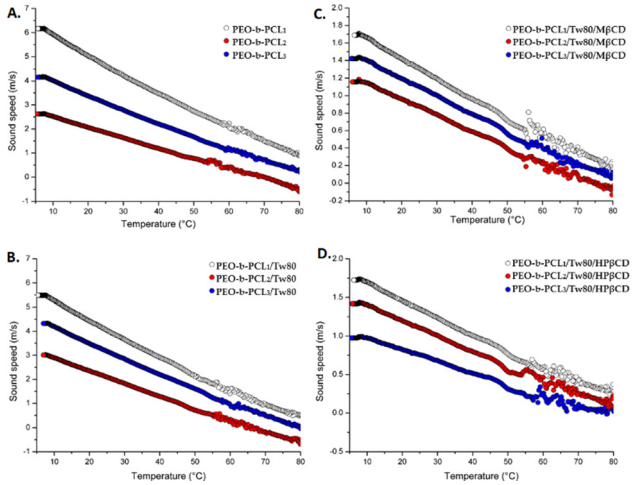

Fig. 4 Sound speed *vs.* temperature for (A) PEO-*b*-PCL_1, PEO-*b*-PCL_2, PEO-*b*-PCL_3, (B) PEO-*b*-PCL_1/Tw80, PEO-*b*-PCL_2/Tw80, PEO-*b*-PCL_3/Tw80, (C) PEO-*b*-PCL_1/Tw80/MβCD, PEO-*b*-PCL_2/Tw80/MβCD, PEO-*b*-PCL_3/Tw80/MβCD, and (D) PEO-*b*-PCL_1/Tw80/HPβCD, PEO-*b*-PCL_2/Tw80/HPβCD, PEO-*b*-PCL_3/Tw80/HPβCD formulations.

These results recorded values in the range of 53–54 °C for the systems containing PEO-*b*-PCL_1 and PEO-*b*-PCL_3, and also 49–55 °C for the systems comprised of PEO-*b*-PCL_2. As for mDSC, the observed transitions are only slightly appreciated by HR-US, confirming the complementary nature of these techniques in investigating the thermal transitions of liquid-dispersed colloidal systems.

Finally, we should recapitulate that the above techniques indicated the existence of a wide variety of interactions between the compounds that were attributed to the self-assembly process. The presence of the non-ionic Tw80 influenced appreciably the thermotropic behavior of the polymer. The interactions improved after the incorporation of MβCD or HPβCD resulted in the solubilization of the prepared systems.

It is obvious that the results taken from mDSC and HR-US presented some dissimilarities between the thermotropic characteristics of the prepared systems in comparison to those obtained by DSC. These differences are strongly associated with the different heating rates of the methods used as well as the different states of the systems. In DSC, we investigated the interactions between the pure compounds in the solid state, whereas in mDSC and HR-US techniques, the systems were in the liquid dispersed colloidal state, having the ability to self- or co-assemble. Thus, the steric interactions due to PEO hydrophilic chains contributed to the production of systems with a different thermal behavior in the dispersed liquid state.

3.6. Tensiometric analysis results

The calculated surface tension values (γ) for the prepared systems are also presented in Table 2. The parameter γ is a measure of the effectiveness of a surfactant to decrease air–water surface tension. Regarding the air–water surface tension values, it was calculated that the more hydrophobic the polymer was, the higher the measured surface tension was. Indeed, these values were 47, 52, and 53 mN m^{-1} for PEO-*b*-PCL_1, PEO-*b*-PCL_2, and PEO-*b*-PCL_3, respectively. The addition of Tw80 caused a decrease in surface tension values in the range of 6 to 12 mN m^{-1}, with the most significant decrease observed for the PEO-*b*-PCL_3 block copolymer. On the one hand, the incorporation of MβCD into the binary systems led to a further slight decrease in surface tension values for systems prepared with PEO-*b*-PCL_1 (3 mN m^{-1}) and PEO-*b*-PCL_2 (1 mN m^{-1}). On the other hand, it caused a slight increase in γ values for the system prepared with PEO-*b*-PCL_3 (2 mN m^{-1}). Regarding the addition of HPβCD, all systems remained largely unaffected by the presence of HPβCD.

Comparing the data published in the literature for Tw80, critical micelle concentrations were reported in a broad range. For instance, Garidel *et al.*[43] reported the critical micelle concentration (CMC) for Tw80 around 7–16 μM, whereas Rehman *et al.*[44] demonstrated its value equal to 19 μM. This variability in the CMC values may be attributed to the fact that the used Tw80 was supplied from different manufacturers and the experiments were conducted under dissimilar conditions.[43]

As described in the literature,[44] critical aggregation concentration (CAC) and CMC are the critical values that characterize the binding mechanism of block copolymer–surfactant systems. CAC is the critical concentration of surfactant; above this, the complexation of the diblock copolymer with surfactant takes place, whereas CMC corresponds to the value at which saturation of the block copolymer is achieved by surfactant molecules. In values of concentration lower than CAC, the hydrophilic PEO chains of surfactants could adsorb on the block copolymer surface *via* electrostatic interactions that are developed due to the "cooperativity" in binding of Tw80 molecules, leading to an increase in the surface charge on the block copolymer surface and the further complexation of the compounds. Subsequently, the stability of the system is achieved. When the concentration of surfactant is higher than CAC, the formation of micelles is observed, and micelles are attached to the diblock copolymer *via* hydrophobic interactions.[44] Concerning all the above, we can extrapolate the information that the concentrations of PEO-*b*-PCL diblock copolymers used for tensiometric analyses were higher than CAC. Consequently, the possible formation of micelles *via* hydrophobic bonds between Tw80 and PEO-*b*-PCL diblock copolymers could be achieved.

To conclude, binary and ternary systems of PEO-*b*-PCL block copolymers with the presence of both surfactant and βCD derivatives displayed similar profiles, highlighting the improved interactions between the materials of each system.

3.7. Morphological characterization of hybrid systems

As visualized by cryo-TEM images of hybrid formulations containing PEO-*b*-PCL_1 polymer, a variety of different structures was observed (Fig. 5).

Among these structures, irregular, close-to-spherical particles (red arrows) were detected, displaying irregular surfaces and sizes ranging from 100–200 nm and 120–170 nm for systems with MβCD and HPβCD, respectively. The observed systems' shape asymmetry may be influenced by the rather

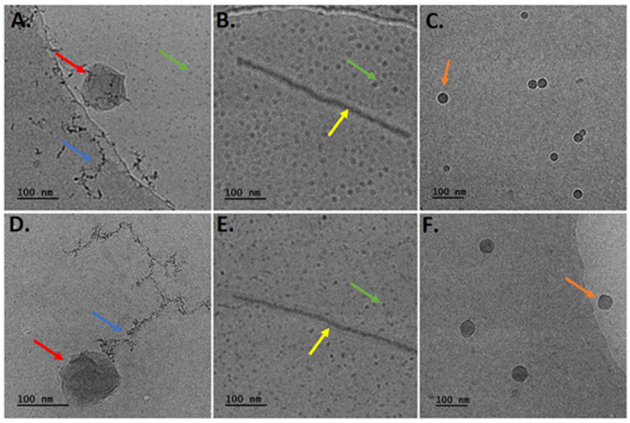

Fig. 5 Cryo-TEM images of PEO-*b*-PCL_1/Tw80/MβCD (A)–(C) and PEO-*b*-PCL_1/Tw80/HPβCD (D)–(F) systems.

high colloidal concentration, equal to 10 mg mL^{-1}. It may also be attributed to the non-uniform incorporation of block copolymer chains within the nanostructures, leading to regions enriched in block copolymer chains.[2] In both systems, small spherical particles (4–10 nm) were observed (indicated by the green arrows). These particles exhibited a tendency to aggregate and form threadlike structures (blue arrows). Besides these three types of self-assemblies, the co-assembly process and co-organization of the different components led to the formation of large worm-like structures with a thickness of 15 nm. The lengths of these structures were found to be in the range of 100–500 nm and 120–660 nm for hybrid systems containing MβCD and HPβCD, respectively. Finally, spherical particles (orange arrows) were observed. Their diameter for PEO-*b*-PCL_1/Tw80/MβCD was found to be around 20–50 nm with cryo-TEM, whereas the corresponding ones for PEO-*b*-PCL_1/Tw80/HPβCD presented similar sizes (15–60 nm). These results are in agreement with those measured by DLS. Indeed, the populations of particles measured by DLS (Table 1) are included in the population observed in cryo-TEM images.

Concerning the hybrid systems involving PEO-*b*-PCL_2 copolymer in combination with Tw80 and either MβCD or HPβCD, two different structures were detected in cryo-TEM images (Fig. 6). Notably, small spherical particles, exhibiting dimensions equal to 4–10 nm and 4–25 nm, and elongated rod-like formations characterized by a thickness ranging from 10–15 nm, with corresponding lengths of 80–930 nm and 150–800 nm for the PEO-*b*-PCL_2/Tw80/MβCD and PEO-*b*-PCL_2/Tw80/HPβCD, respectively.

The same type of objects was also identified in cryo-TEM images for ternary systems containing PEO-*b*-PCL_3 (Fig. 7). In comparison to the PEO-*b*-PCL_2 systems, the population of small spherical particles exhibited larger dimensions, falling within the range of 4 to 50 nm. A clear layer with a thickness of approximately 6 nm (red arrows) was distinguished. Additionally, rod-shaped entities (yellow arrows) were also present in the images. These rods displayed a uniform thickness of 10–15 nm and measured lengths of 170–730 nm for the PEO-*b*-PCL_3/Tw80/MβCD system and 150–800 nm for the PEO-*b*-PCL_3/Tw80/HPβCD system.

It is obvious that the structures observed in cryo-TEM images display size discrepancies when compared to measurements derived from intensity-weighted results in DLS. While both techniques serve the purpose of analyzing particle size, they are grounded in fundamentally distinct principles, leading to variations in the particle size measurements they provide. Cryo-TEM has a unique advantage as it allows for the direct imaging of colloids in their vitrified, frozen-hydrated state after

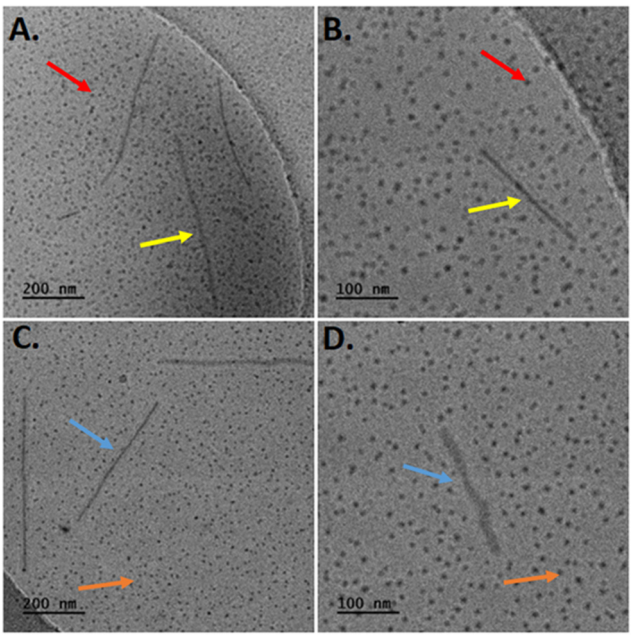

Fig. 6 Cryo-TEM images of PEO-*b*-PCL_2/Tw80/MβCD (A) and (B) and PEO-*b*-PCL_2/Tw80/HPβCD (C) and (D) systems.

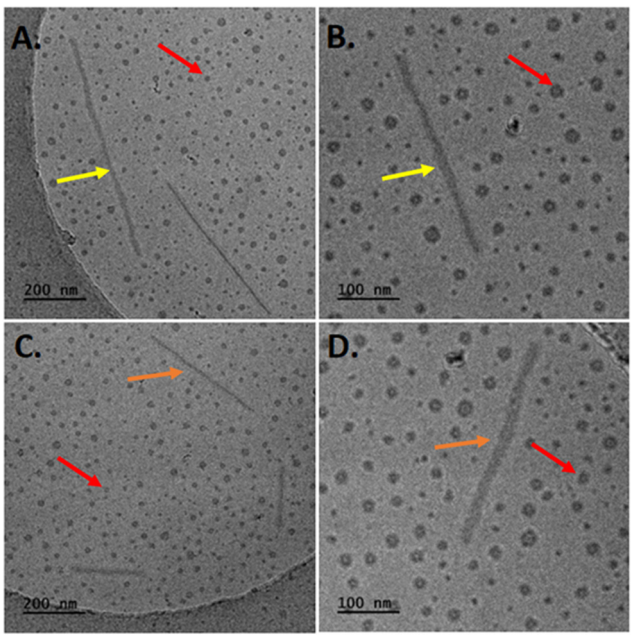

Fig. 7 Cryo-TEM images of PEO-*b*-PCL_3/Tw80/MβCD (A, B) and PEO-*b*-PCL_3/Tw80/HPβCD (C, D) systems.

plunge freezing of dispersions, reflecting the size of the solid state of the particles. This approach closely mimics the colloids' natural state and provides valuable insights into their internal and three-dimensional structure, as demonstrated in the work of Mulet *et al.*[45] In contrast, DLS measures the particle size of hybrid colloidal dispersions in a solution state, and it is associated with the self-assembly phenomena and with the attractive and repulsive interactions of each particle with its neighbouring ones.[2,45,46]

To conclude, diverse structural variations were noted across the distinct systems. Thus, the hydrophilic/hydrophobic ratio, molecular size, mass ratio, and possibly selective segregation within the hybrid structures are critical factors affecting the self-assembly process and the resulting morphologies. Table 3 summarizes the interactions developed between the materials of ternary systems. The structure of the particles obtained, based on all the results, is illustrated schematically in Fig. 8.

3.8. Cytotoxicity of hybrid colloidal dispersions

The toxicity of mixed amphiphilic systems is of paramount importance, and these results could be useful for gaining information about their possible application as drug delivery platforms for the encapsulation of therapeutic agents in subsequent studies. Numerous factors, including size, shape, and surface modification, are known to affect nanotoxicity and are considered to have a crucial impact on both cell internalization and cytotoxicity.[47] Cell viability was expressed as a percentage (%) of cell viability ± SD between two experiments. The results were subsequently subjected to statistical analysis, as outlined in Section 2.2.13. The toxicity profiles of all prepared systems were tested, and they are depicted in Fig. 9 as the bar diagrams of cell viability *vs.* system concentrations. At first glance, systems containing the HPβCD exhibited the lowest cytotoxicity since even the maximum concentration tested (500 μg mL^{-1}) resulted in cell viability that exceeded 70%. On the contrary, from all the other systems tested, PEO-*b*-PCL_2/Tw80/MβCD appeared to be the most toxic one for HEK-293 cells after the incubation period, as cell viability decreased to less than 50% at the highest concentration.

Furthermore, all systems showed excellent biocompatibility at lower concentrations; cell viability values ranged from 94% to 99% at the concentration of 25 μg mL^{-1} and from 83% to 98% at the concentration of 50 μg mL^{-1}. The cytotoxic profile of all systems was degraded proportionally with the increase in concentration. For example, toxicity studies for the PEO-*b*-PCL_3/Tw80/MβCD system revealed that cell viability at the highest concentrations (500 μg mL^{-1}) was 39%.

Regarding the presence of Tw80 surfactant and PEO-*b*-PCL_3 toxicity profiles presented alterations in the range of 1–7%, with the most evident change observed at the 5th highest concentration. It is observed that although the combination of Tw80 with PEO-*b*-PCL_1 block copolymer caused a decrease in

Table 3 The main interactions developed between the ternary systems' materials

DSC	Possible formation of an inclusion complex: • The hydrophobic chains of polymers (PCL chains) and surfactant with the hydrophobic core of βCD's derivatives. • The hydrophilic outer surface of βCD's derivatives may interact with the hydrophilic parts of amphiphilic polymers (*i.e.*, PEO chains) and surfactant (ethylene oxide subunits). • Hydrogen bonds and van de Waals interactions may contribute to this complexation.
DLS	• No significant differences in particle size among different formulations. • After the addition of the βCD's derivative, the contribution of the hydrophobic component (%wt of PCL) may not be pivotal. • Hydrophilic interactions between compounds appear to dominate.
One-month stability study (DLS)	• Stealth characteristics to a certain extent were provided by the hydrophilic corona that was formed by the PEO chains of PEO-*b*-PCL block copolymers.
Biological stability (DLS)	• Stealth characteristics to a certain extent were provided by the hydrophilic corona that was formed by the PEO chains of PEO-*b*-PCL block copolymers.
mDSC & HR-US	• The hydrophobic PCL chains of polymers and non-polar parts of Tw80 may be incorporated into the hydrophobic core of CDs. • The self-assembly ability of the colloidal dispersions may lead to the enhancement of the water solubility of the systems and consequently to the absence of intense peaks with high enthalpy values in mDSC thermograms in comparison with the systems in the solid state.
Fluorescence spectroscopy (I_1/I_3)	• The presence of CDs caused an enhancement to the systems with the most hydrophobic copolymers (PEO-*b*-PCL_2 and PEO-*b*-PCL_3). These observations indicate a significant influence of hydrophilic interactions among the compounds, presumably facilitated by interactions between the hydrophilic PEO chains of the polymer, the head group of Tw80, and the hydrophilic surface of CDs.
Cryo-TEM images	• Spherical particles and threadlike structures developed due to the aggregation phenomena of the particles. • Shape asymmetry due to high colloidal concentration or to the non-uniform incorporation of block copolymer chains within the nanostructures, leading to regions enriched in block copolymer chains. • Large worm-like structures due to the co-assembly process and co-organization of the different components. • Cryo-TEM images confirm the hypothesis of improved interactions between the compounds in ternary systems. • Hydrogen bonding interactions may easily take place in these systems due to the abundance of hydroxyl, ether, and other groups in the components. • Hydrophobic interactions may also be present and may facilitate their co-assembly into nanostructures.

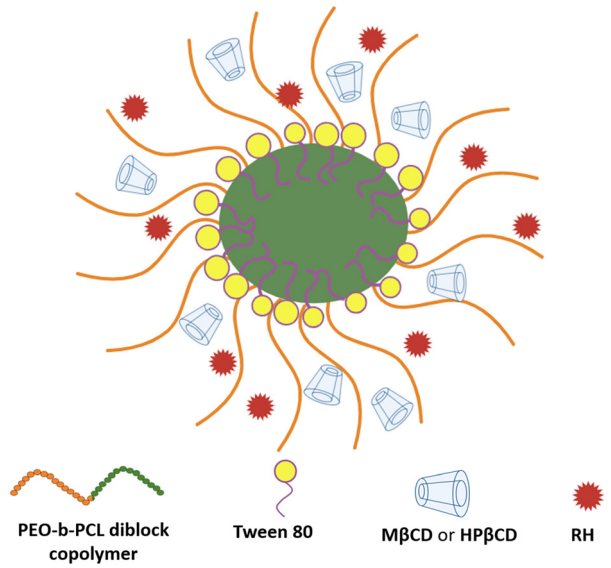

Fig. 8 Schematic illustration of the RH-loaded hybrid particles.

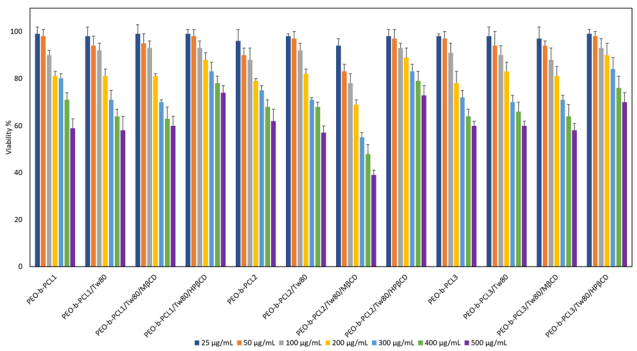

Fig. 9 MTT cell viability assay after 24-h treatment of HEK-293 of colloidal hybrid systems: pure polymer, polymer/Tw80, polymer/Tw80/MβCD, and polymer/Tw80/HPβCD systems. Cell viability is expressed as % cell viability ± SD between two experiments.

viability at concentrations of 300 μg mL^{-1} and 400 μg mL^{-1}, it did not affect the viability of PEO-*b*-PCL$_1$ at the lowest and highest concentrations. In addition to this, Tw80 had a completely different effect on the cytotoxicity behavior of PEO-*b*-PCL$_2$, causing an increase in cell viability at lower concentrations (25 μg mL^{-1}, 50 μg mL^{-1}, 100 μg mL^{-1}, 200 μg mL^{-1}), and simultaneously a slight decrease at concentrations of 300 μg mL^{-1} and 500 μg mL^{-1}. This behavior may be related to the co-operativity of the components driven by their individual and relative amphiphilicity.

We should also point out that the incorporation of HPβCD had a beneficial effect on the cytotoxicity profile of the prepared hybrid systems. That is obvious, as toxicity levels for all systems containing HPβCD exhibited viability that exceeded 70% even at the maximum concentration (500 μg mL^{-1}) investigated. In contrast, the presence of MβCD increased the cytotoxicity of all systems, especially in PEO-*b*-PCL$_2$/Tw80/MβCD hybrid systems, with cell viability at concentrations of 400 μg mL^{-1} and 500 μg mL^{-1} being 48% and 39%, respectively. Indeed, statistical analysis revealed that the systems containing HPβCD exhibited statistically significant cell viability compared to those with MβCD at the concentration of 300 μg mL^{-1} ($p < 0.05$, 95% CI). Regarding PEO-*b*-PCL$_2$, these differences were crucial at all the concentrations tested higher than 50 μg mL^{-1} ($p < 0.05$, 95% CI). According to the European Medical Agency,[48] HPβCD can be used as an excipient in the majority of medicinal products (oral, rectal, dermal, ocular and parenteral), whereas MβCD can be added only in nasal and ocular products. This may be attributed to the fact that HPβCD is considered less toxic under specific dose limits in comparison with MβCD, which is in accordance with the more beneficial cell viability of the hydroxyl-propyl derivative of βCD that is presented in our results obtained by the MTT assay.

The comparison among hybrid systems utilizing different PEO-*b*-PCL polymers indicated that PEO-*b*-PCL$_2$/Tw80/MβCD exhibited lower cell viability than PEO-*b*-PCL$_1$/Tw80/MβCD and PEO-*b*-PCL$_3$//Tw80/MβCD ($p < 0.05$, 95% CI). The same observations may be underlined after the comparison of the PEO-*b*-PCL$_2$/Tw80/HPβCD with the PEO-*b*-PCL$_3$/Tw80/HPβCD system at concentrations of 300 and 500 μg mL^{-1} ($p < 0.05$, 95% CI).

Based on the findings of the MTT assay, the tested formulations can be deemed biocompatible at low concentrations (25 and 50 μg mL^{-1}), with their cell viability exceeding 80%. However, as the dose of the formulations was increased, a dose-dependent increase in cytotoxicity was observed, with the degree of cytotoxicity varying depending on their composition. It is noteworthy that the hybrid systems containing HPβCD are considered non-toxic, even at high concentrations of 100, 200, and 300 μg mL^{-1}. Consequently, all systems showed dose-dependent and material-dependent toxicity on HEK293 cell lines. Finally, the selected results from toxicity studies will act as a road map for the evaluation of the prepared systems as carriers for drug delivery purposes.

3.9. Physicochemical characterization of RH systems

Hybrid RH systems were prepared at weight ratios of 10 : 1 and 10 : 5 using the protocol outlined in Section 2.2.2. DLS measurements were conducted on the first day of their preparation. All results taken are reported in Table S4 and depicted in Fig. S5 (ESI†).

Regarding the PEO-*b*-PCL$_1$/Tw80/MβCD/RH and PEO-*b*-PCL$_1$/Tw80/HPβCD/RH systems, an increase in PDI was observed in all the tested formulations compared to the systems without RH. This observation is also visually supported by the broader curves depicted in Fig. S5 (ESI†). Two populations were identified, and the percentage of the appearance of the population with the lower R_h increased by 13%. The population with the larger particles presented a decrease in R_h in the range of 31–41 nm and approximately 15 nm for the RH systems with weight ratios of 10 : 1 and 10 : 5, respectively.

In the case of PEO-*b*-PCL$_2$/Tw80/MβCD/RH systems, the PDI of the systems remained almost unaffected. In both RH-loaded

systems, a notable increase was observed in the prevalence of a population comprised of smaller particles. This increase amounted to 41% and 47% for the respective concentrations of RH, 1 mg mL^{-1} and 5 mg mL^{-1}. Furthermore, it was observed that the different concentrations of RH affected the dimensions of the particles. On the one hand, the incorporation of 1 mg mL^{-1} of RH resulted in a decrease in R_h of the larger population by 23 nm. On the other hand, the inclusion of 5 mg mL^{-1} of RH led to an increase in the R_h of the same population by 30 nm. The incorporation of RH in the PEO-*b*-PCL_2/Tw80/HPβCD inclusion complex resulted in the substitution of the previously existing dual populations, characterized by dimensions of 14 nm and 136 nm, with a single population with high heterogeneity. Concurrently, the R_h exhibited an alteration, measuring 18 nm at the concentration of RH equal to 1 mg mL^{-1} and 23 nm when the RH concentration was raised to 5 mg mL^{-1}.

As presented in Table S5 (ESI†), DLS analysis for PEO-*b*-PCL_3/Tw80/MβCD revealed the existence of two distinct populations. The most dominant one (comprising 62% of the distribution) exhibited an R_h of 96 nm, and the other one was equal to 19 nm. It is noted that the addition of RH in both concentrations led to the replacement of these populations by a single, homogenous population with a diminished R_h of 25 nm. Regarding the last formulations tested, namely the PEO-*b*-PCL_3/Tw80/HPβCD/RH systems, a notable reduction in the PDI was evident when contrasted with the pristine system. The highest reduction was observed in the RH-loaded system with the highest concentration of RH. In the case of the weight ratio of 10 : 1, the results revealed a dominant population of 71% with an R_h of around 22 nm. Additionally, a secondary population with an R_h of 221 nm was also identified (ESI,† Table S5). Regarding the weight ratio of 10 : 5, the DLS analysis showed that the two different populations observed in the size distribution diagram of PEO-*b*-PCL_3/Tw80/HPβCD were replaced by a single homogenous population, presenting an R_h of 23 nm.

In summary, these findings suggest that the incorporation of RH into the hybrid systems influenced each system in a different way. Indeed, alterations in particle size and polydispersity value were observed based on the composition of the systems as well as the specific weight ratios of the components. These disparities could potentially be attributed to different interactions and co-assembly behaviors among the components.

3.10. RH content in the prepared systems

RH content ranged from 91.80% to 109.77% (0.046 to 0.055 mg of RH, respectively) of the theoretical loading dose (observed difference less than 10%), and standard deviations varied from 0.62% to 7.55%.

3.11. RH' s release from the formulation by *in vitro* diffusion experiments

In vitro release tests for RH from the prepared formulations (F1–F12) and RH solution (0.5 mg mL^{-1}, PBS pH = 5.6) were conducted using Franz cells and regenerated cellulose membranes with specific pore sizes as diffusion barriers. The 1000 Da molecular weight cutoff allowed free RH to pass through while blocking potential interactions among formulation components. The mass balance results, as shown in Table 4, encompass the total permeated amount, the calculated RH quantity in the donor compartment at the experiment's conclusion, and the RH amount remaining in the membrane at the end of the experiment. The cumulative amount and the percentage of the loaded dose diffused for two different concentrations of RH. Fig. S6, S7, and S8 (ESI†) correspond to the RH-loaded ternary systems for PEO-*b*-PCL_1, PEO-*b*-PCL_2, and PEO-*b*-PCL_3, respectively. All samples were analyzed using the HPLC-PDA method described in Section 2.2.11.

A comparison of the % dose permeated of RH from the tested formulations with the RH solution indicates notable statistical differences ($p < 0.05$, 95% CI) in some cases. Specifically, formulations F9, F10, and F11 exhibited a significantly lower release profile compared to the control solution during the experiment. Conversely, the remaining formulations did not exhibit any significant differences compared to the control solution. Notably, among all the tested formulations, F8 exhibited the most closely resembling release profile to that of the RH solution.

For systems containing PEO-*b*-PCL_1, the *in vitro* release profiles of RH show no significant differences (ESI,† Fig. S6).

Table 4 Percentage (%) RH loading dose permeated for the tested formulation, mass balance of RH in each formulation, and membrane retention data of each formulation expressed as the percent (%) of the loading dose retained by the cellulose membrane (mean ± SD, n = 3)

Formulation		w/w	RH permeated (% loading)	Mass balance	% of the dose retained by the cellulose membrane
F1	(PEO-*b*-PCL_1/Tw80/MβCD)/RH	10 : 1	90.86 ± 3.60	92.20 ± 4.60	0.60 ± 0.18
F2	(PEO-*b*-PCL_1/Tw80/MβCD)/RH	10 : 5	90.41 ± 4.86	94.53 ± 3.80	0.50 ± 0.05
F3	(PEO-*b*-PCL_1/Tw80/HPβCD)/RH	10 : 1	91.08 ± 2.21	93.48 ± 2.73	0.46 ± 0.09
F4	(PEO-*b*-PCL_1/Tw80/HPβCD)/RH	10 : 5	92.37 ± 4.46	95.80 ± 4.15	0.46 ± 0.19
F5	(PEO-*b*-PCL_2/Tw80/MβCD)/RH	10 : 1	88.65 ± 7.08	91.18 ± 7.67	0.37 ± 0.03
F6	(PEO-*b*-PCL_2/Tw80/MβCD)/RH	10 : 5	99.76 ± 2.29	102.43 ± 2.16	0.52 ± 0.09
F7	(PEO-*b*-PCL_2/Tw80/HPβCD)/RH	10 : 1	93.72 ± 2.43	96.37 ± 2.37	0.39 ± 0.12
F8	(PEO-*b*-PCL_2/Tw80/HPβCD)/RH	10 : 5	100.68 ± 5.83	104.64 ± 6.43	0.35 ± 0.17
F9	(PEO-*b*-PCL_3/Tw80/MβCD)/RH	10 : 1	89.67 ± 1.69	93.98 ± 3.17	0.63 ± 0.27
F10	(PEO-*b*-PCL_3/Tw80/MβCD)/RH	10 : 5	89.79 ± 2.72	93.79 ± 2.63	0.61 ± 0.16
F11	(PEO-*b*-PCL_3/Tw80/HPβCD)/RH	10 : 1	84.25 ± 3.05	87.94 ± 3.63	0.66 ± 0.12
F12	(PEO-*b*-PCL_3/Tw80/HPβCD)RH	10 : 5	92.88 ± 0.74	96.48 ± 0.52	0.53 ± 0.07
Control	RH solution (0.5 mg mL^{-1})	—	96.93 ± 2.11	99.72 ± 1.99	0.37 ± 0.04

However, it is worth noting that after the first hour of the experiment, F2 and F4 formulations (containing either MβCD or HPβCD, respectively, and RH at its higher concentration) exhibit higher cumulative amounts of RH compared to F1 and F3 formulations (containing either MβCD or HPβCD, respectively, and RH at its lower concentration). The percentage of RH released remains nearly identical across all formulations. Regarding the PEO-*b*-PCL_2 systems (ESI,† Fig. S7), the F8 formulation (containing HPβCD and RH at its higher concentration) demonstrated the highest RH permeation per unit area, following the sequence F8 > F6 > F5 > F7. Statistical distinctions were observed upon evaluating formulations F5 and F8 at the time points of 60 min and 90 min, as well as in the comparison between formulations F7 and F8 at 45 and 60 min. This observation reveals that, for the same RH content, formulations containing HPβCD perform better *in vitro* release profiles than those containing MβCD. In the case of the PEO-*b*-PCL_3 systems (ESI,† Fig. S8), RH displayed the most effective release profile in the F12 formulation (containing HPβCD, and RH at its higher concentration). Based on these results, it can be concluded that RH demonstrates superior *in vitro* release characteristics in systems containing HPβCD at a RH concentration of 5 mg mL^{-1}. The permeation profiles through regenerated cellulose membranes for the colloidal dispersion of RH-loaded PEO-*b*-PCL_1, PEO-*b*-PCL_2, and PEO-*b*-PCL_3 hybrid systems are illustrated in Fig. S6–S8 (ESI†), respectively.

When comparing these systems (F4, F8, and F12), it becomes evident that F4 and F12 exhibit nearly identical percentages of the dose permeated during the experiment. Statistical analysis did not reveal any significant differences ($p > 0.05$, 95% CI). The F8 formulation exhibits a slightly higher percentage of RH permeated at all times. The most notable disparities were detected between F4 and F8 at 45 min and 210 min ($p < 0.05$, 95% CI), as well as between F8 and F12 at 45 min ($p < 0.05$, 95% CI) after the start of the experiment.

Applying eqn (1) up to 120 min in the plots of the amount of RH (Q) permeated per unit area (A) *versus* time plots in Fig. 10A (since a plateau is reached after that time in all cases), the flux for each prepared formulation was calculated and found to vary from $4.2 \times 10^{-4} \pm 7.0 \times 10^{-5}$ to $6.1 \times 10^{-4} \pm 8.0 \times 10^{-5}$ μg cm^{-2} min^{-1}. In addition, the R^2 values, varying from 0.872 ± 0.009 to 0.949 ± 0.005, reveal the linear increase in Q/A with time, which is consistent with the first-order kinetics of the diffusion process. The flux values ± SD of each formulation are included in Table S5 of the ESI.†

Moreover, the quantification of RH remaining in the cellulose membrane revealed that 0.37 ± 0.03 to 0.66 ± 0.12% to of the loading doses are retained on average by the artificial membrane. Membrane retention data for each formulation, expressed as the percent (%) of the loading dose retained by the cellulose membrane ± SD, are included in Table 4.

In all formulations, over 50% of RH permeated through the cellulose membrane within the first hour of the experiment. It should also be noted that F8 (containing HPβCD and RH at its higher concentration) exhibited the highest mass balance (104.64 ± 6.43) and percentage of RH permeated per unit area over time (100.68 ± 5.83), whereas F11 (containing HPβCD and RH at its lower concentration) had the lowest values (87.93 ± 3.63 and 84.25 ± 3.05, respectively).

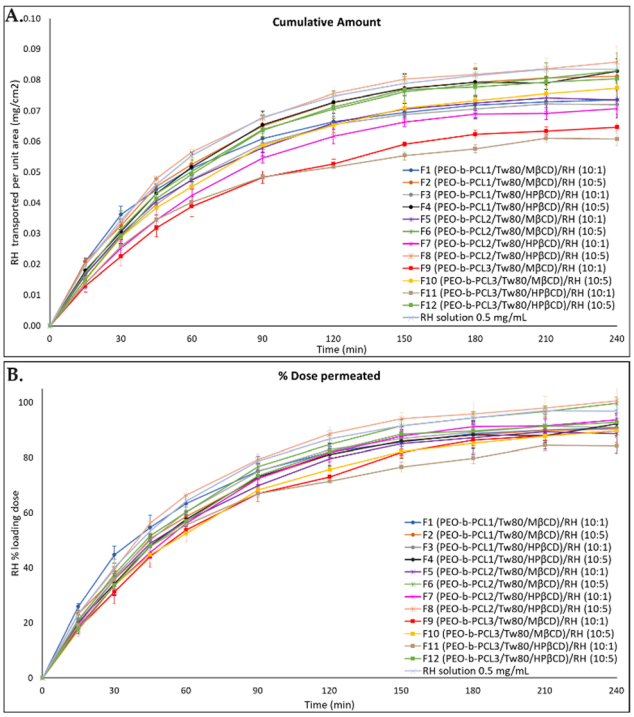

Fig. 10 Permeation profiles through regenerated cellulose membranes for the colloidal dispersion of RH-loaded PEO-*b*-PCL hybrid systems at the weight ratios of 10 : 1 and 10 : 5 at the buffer solution pH = 5.6 in comparison to RH solution (0.5 mg mL^{-1}, PBS pH = 5.6), expressed as (A) quantity permeated per unit area (mean ± SD, n = 3) and (B) % loading dose permeated for the tested formulation (mean ± SD, n = 3).

Overall, throughout the experiment, RH's release from all formulations progressively increased, as illustrated in Fig. 10, and it maintained a notably high mass balance. The beneficial release profile can be attributed to the interactions among the components of the formulation, which effectively facilitated the drug's diffusion into the membrane. The release profile of RH was influenced by its concentration, with higher cumulative amounts observed in all formulations when the weight ratio of nanosystem/RH was 10 : 5.

The *in vitro* findings also suggest that, among the prepared formulations, RH exhibited superior *in vitro* release characteristics when incorporated in systems containing HPβCD. This underlines the impact of varying weight ratios of components and their compositions on the release profile of RH from the formulations. Hence, it appears that these formulations (F4, F8, and F12) manifest a superior release profile, with F8 being the most favorable, resembling the profile obtained with the RH solution (0.5 mg mL^{-1}, PBS pH = 5.6). These characteristics potentially facilitate the efficient delivery of RH from the nasal route, probably resulting in a quicker onset of action in the brain. As previously discussed, RH is classified as a BCS class III drug (high water solubility and low permeability), which resulted in no statistically significant differences between the release profiles of the prepared formulations. However, the

promising results, regarding mainly the formulations containing HPβCD, encouraged the ongoing further research with *ex vivo* permeation experiments. The results of these experiments will enable the discrimination between the mucosal permeability of the different formulations and the selection of the optimum formulation to be further used for *in vivo* nasal administration, which will support the results of the present work.

4. Conclusions

In this study, hybrid biomimetic and bio-inspired systems composed of PEO-*b*-PCL block copolymers, Tw80, and derivatives of βCD, namely MβCD and HPβCD, were prepared. This is the first report described in the literature in which the combination of block copolymers with CDs was studied *via* different thermal and physicochemical techniques. DSC experiments revealed a wide range of interactions between the compounds, which were confirmed by the application of mDSC and HR-US techniques. The stability of the colloidal dispersions may be attributed to the steric repulsion of the hydrophilic polymeric blocks, which is a property provided by the hydrophilic corona of the PEO chains of each polymer. This occurred despite the fact that the z-potential values of most systems were only slightly negative. Concerning the surface tension of the systems, it was determined that the more hydrophobic the polymer was, the higher the measured surface tension would be, whereas the presence of both surfactant and βCD derivatives affected each PEO-*b*-PCL block copolymer in a noticeably different way. Regarding the cytotoxicity profile of the prepared systems, based on the MTT assay studies, all samples showed dose-dependent toxicity on the HEK293 cell lines. *In vitro* diffusion experiments under pH and temperature conditions that mimic those of the human nasal cavity consistently demonstrated an effective release of RH from the formulations, with a mass balance exceeding 90% in most cases. Particularly, systems containing a 5 mg mL^{-1} concentration of RH and HPβCD exhibited superior *in vitro* release characteristics resembling those of the RH solution (0.5 mg mL^{-1}, PBS pH = 5.6). These promising results enhance the potential of these hybrid, cutting-edge systems for nasal drug delivery applications. Ongoing research will assess *ex vivo* permeation through the nasal mucosa of rabbits. Subsequently, the *in vivo* pharmacokinetic profiles in both serum and brain will be investigated following the nasal administration of the optimally developed products.

Abbreviations

APIs	Active pharmaceutical ingredients
BCS	Biopharmaceutical classification system
CI	Confidence interval
CAC	Critical aggregation concentration
CMC	Critical micelle concentration
CDs	Cyclodextrins
DSC	Differential scanning calorimetry
A	Diffusion area
DLS	Dynamic light scattering
ELS	Electrophoretic light scattering
ΔH	Enthalpy
FBS	Fetal bovine serum
J	Flux
HPLC	High-performance liquid chromatography
HR-US	High-resolution ultrasound spectroscopy
$\Delta T_{1/2}$	Half width at half peak height of the transition
HPβCD	Hydroxy-propyl-β-CD
R_h	Hydrodynamic radius
IQR	Interquartile range
T_m	Main transition temperature
MβCD	Methyl-β-CD
mDSC	Microcalorimetry
MW	Molecular weight
PBS	Phosphate buffer solution
PCL	Poly-ε-caprolactone
PEO	Polyethylene oxide
PEO-*b*-PCL	Poly(ethylene-oxide)-*b*-poly(ε-caprolactone)
PDI	Polydispersity index
RH	Ropinirole hydrochloride
SD	Standard deviations
Tw80	Tween 80
z-potential	Zeta potential

Author contributions

Conceptualization, N. P., S. P. and G. V.; methodology, E.-M. S., N. P., S. P. and G. V.; validation, E.-M. S., D. R. P., A. F. and P. P.; formal analysis, E.-M. S., D. R. P. and A. F.; investigation, E.-M. S., N. P., S. P. and G. V.; resources, N. P., S. P. and G. V.; data curation, E.-M. S., P. P., N. L., M. G., G. B. and B. T.; writing—original draft preparation, E.-M. S.; writing—review and editing, N. P., D. R. P., A. F., P. P., S. P., M. G., G. B., B. T., N. L. and G. V.; visualization, E.-M. S.; supervision, N. P., S. P. and G. V.; project administration, N. P., S. P. and G. V. All authors have read and agreed to the published version of the manuscript.

Conflicts of interest

The authors report no conflict of interest.

Acknowledgements

We would like to thank Costas Demetzos and Paraskevas Dallas for providing access to the equipment of their laboratories to conduct the DSC and diffusion experiments, respectively, as well as Dimitrios Selianitis for his valuable contribution to the fluorescence spectroscopy measurements. Elmina-Marina Saitani would like to acknowledge the Bodossaki Foundation for the PhD scholarship.

References

1 N. Pippa, S. Pispas and C. Demetzos, *Curr. Pharm. Des.*, 2016, **22**, 2788–2795.
2 N. Pippa, N. Naziris, D. Stellas, C. Massala, K. Zouliati, S. Pispas, C. Demetzos, A. Forys, A. Marcinkowski and B. Trzebicka, *Colloids Surf., B*, 2019, **177**, 338–345.
3 S. Pispas and E. Sarantopoulou, *Langmuir*, 2007, **23**, 7484–7490.
4 A. Mahmud, X.-B. Xiong and A. Lavasanifar, *Macromolecules*, 2006, **39**, 9419–9428.
5 F. Kareem, A. M. Bhayo, M. Imran, M. R. Shah, K. M. Khan and M. I. Malik, *J. Appl. Polym. Sci.*, 2019, **136**, 47769.
6 M. Shahin and A. Lavasanifar, *Int. J. Pharm.*, 2010, **389**, 213–222.
7 X. Wei, C. Gong, M. Gou, S. Fu, Q. Guo, S. Shi, F. Luo, G. Guo, L. Qiu and Z. Qian, *Int. J. Pharm.*, 2009, **381**, 1–18.
8 P. Grossen, D. Witzigmann, S. Sieber and J. Huwyler, *J. Controlled Release*, 2017, **260**, 46–60.
9 T. K. Dash and V. B. Konkimalla, *Mol. Pharmaceutics*, 2012, **9**, 2365–2379.
10 E. Khodaverdi, Z. Heidari, S. A. Tabassi, M. Tafaghodi, M. Alibolandi, F. S. Tekie, B. Khameneh and F. Hadizadeh, *AAPS PharmSciTech*, 2015, **16**, 140–149.
11 M. Valero, I. Grillo and C. A. Dreiss, *J. Phys. Chem. B*, 2012, **116**, 1273–1281.
12 R. M. Haley, R. Gottardi, R. Langer and M. J. Mitchell, *Drug Delivery Transl. Res.*, 2020, **10**, 661–677.
13 Y. Cirpanli, E. Bilensoy, A. Lale Doğan and S. Caliş, *Eur. J. Pharm. Biopharm.*, 2009, **73**, 82–89.
14 D. Zhang, P. Lv, C. Zhou, Y. Zhao, X. Liao and B. Yang, *Mater. Sci. Eng., C*, 2019, **96**, 872–886.
15 L. Rita, T. Amit, G. Chandrashekhar and P. K. M. Kundnani, *Int. J. Res. Ayurveda Pharm.*, 2011, **2**, 1520–1526.
16 E.-M. Saitani, D. Selianitis, N. Pippa, S. Pispas and G. Valsami, *Nanotechnol. Rev.*, 2024, **13**(1), DOI: 10.1515/ntrev-2023-0204.
17 A. J. Poudel, F. He, L. Huang, L. Xiao and G. Yang, *Carbohydr. Polym.*, 2018, **194**, 69–79.
18 X. Li, H. Liu, J. Li, Z. Deng, L. Li, J. Liu, J. Yuan, P. Gao, Y. Yang and S. Zhong, *Colloids Surf., B*, 2019, **183**, 110425.
19 N. Kuplennik and A. Sosnik, *Molecules*, 2019, **24**, 2715.
20 X. Li, Y. Yu, Q. Ji and L. Qiu, *Nanomedicine*, 2015, **11**, 175–184.
21 Y. Gao, G. Li, Z. Zhou, L. Guo and X. Liu, *Colloids Surf., B*, 2017, **160**, 364–371.
22 L. Zhang, J. Lu, Y. Jin and L. Qiu, *Colloids Surf., B*, 2014, **122**, 260–269.
23 E. Barcia, L. Boeva, L. García-García, K. Slowing, A. Fernández-Carballido, Y. Casanova and S. Negro, *Drug Delivery*, 2017, **24**, 1112–1123.
24 N. Pippa, E. Kaditi, S. Pispas and C. Demetzos, *Soft Matter*, 2013, **9**, 4073–4082.
25 A. Chroni, V. Chrysostomou, A. Skandalis and S. Pispas, *Methods Mol. Biol.*, 2021, **2207**, 71–83.
26 A. Chroni, T. Mavromoustakos and S. Pispas, *Nanomaterials*, 2020, **10**, 1872.
27 G. Leonis, E. Christodoulou, D. Ntountaniotis, M. V. Chatziathanasiadou, T. Mavromoustakos, N. Naziris, M. Chountoulesi, C. Demetzos, G. Valsami, D. E. Damalas, A. G. Tzakos, N. S. Thomaidis, V. Karageorgos and G. Liapakis, *Chem. Biol. Drug Des.*, 2020, **96**, 668–683.
28 D. Perinelli, L. Casettari, M. Cespi, F. Fini, D. Man, G. Giorgioni, S. Canala, J. Lam, G. Bonacucina and G. Palmieri, *Colloids Surf., A*, 2016, **492**, 38–46.
29 O. Kontogiannis, D. Selianitis, D. R. Perinelli, G. Bonacucina, N. Pippa, M. Gazouli and S. Pispas, *Int. J. Mol. Sci.*, 2022, **23**, 13814.
30 L. de Souza Teixeira, T. Vila Chagas, A. Alonso, I. Gonzalez-Alvarez, M. Bermejo, J. Polli and K. R. Rezende, *Pharmaceutics*, 2020, **12**, 988.
31 E. M. Saitani, N. Pippa, D. R. Perinelli, A. Forys, P. Papakyriakopoulou, N. Lagopati, G. Bonacucina, B. Trzebicka, M. Gazouli, S. Pispas and G. Valsami, *Int. J. Mol. Sci.*, 2024, **25**, 1162.
32 M. L. L. Pérez-González, C. H. González-de la Rosa, G. Pérez-Hernández and H. I. Beltrán, *Colloids Surf., B*, 2020, **187**, 110758.
33 C. M. De Melo, A. L. Da Silva, K. R. De Melo, P. C. D. Da Silva, M. L. de Souza, A. L. M. D. de Sousa, M. M. Rabello, L. M. C. Véras, L. A. Rolim and P. J. Rolim Neto, *J. Drug Delivery Sci. Technol.*, 2021, **65**, 102658.
34 K. Pramod, C. Suneesh, S. Shanavas, S. Hussain and J. Ali, *J. Anal. Sci. Technol.*, 2015, **6**, 34.
35 M. Lazaratos, K. Karathanou, E. Mainas, A. Chatzigoulas, N. Pippa, C. Demetzos and Z. Cournia, *Biochim. Biophys. Acta, Gen. Subj.*, 2020, **1864**, 129671.
36 J. Zhang and P. X. Ma, *Angew. Chem., Int. Ed.*, 2009, **48**, 964–968.
37 A. Zafar, N. K. Alruwaili, S. S. Imam, O. A. Alsaidan, F. K. Alkholifi, K. S. Alharbi, E. M. Mostafa, A. S. Alanazi, S. J. Gilani, A. Musa, S. Alshehri, A. Rawaf and A. Alquraini, *Pharmaceutics*, 2021, **13**, 1997.
38 N. Pippa, D. Stellas, A. Skandalis, S. Pispas, C. Demetzos, M. Libera, A. Marcinkowski and B. Trzebicka, *Eur. J. Pharm. Biopharm.*, 2016, **107**, 295–309.
39 R. R. Sawant and V. P. Torchilin, *AAPS J.*, 2012, **14**, 303–315.
40 N. Pippa, E. Deli, E. Mentzali, S. Pispas and C. Demetzos, *J. Nanosci. Nanotechnol.*, 2014, **14**, 5676–5681.
41 D. Selianitis and S. Pispas, *Polym. Chem.*, 2021, **12**, 6582–6593.
42 D. R. Perinelli, M. Cespi, F. Rendina, G. Bonacucina and G. F. Palmieri, *Int. J. Pharm.*, 2019, **560**, 385–393.
43 P. Garidel, M. Blech, J. Buske and A. Blume, *J. Pharm. Innov.*, 2020, **16**, 726–734.
44 N. Rehman, H. Ullah, S. Alam, A. K. Jan, S. W. Khan and M. Tariq, *J. Mater. Environ. Sci.*, 2017, **8**, 1161–1167.
45 X. Mulet, B. J. Boyd and C. J. Drummond, *J. Colloid Interface Sci.*, 2013, **393**, 1–20.
46 Z. Zhou, F. Guo, N. Wang, M. Meng and G. Li, *Int. J. Biol. Macromol.*, 2018, **116**, 911–919.
47 S. Salatin, S. M. Dizaj and A. Y. Khosroushahi, *Cell Biol. Int.*, 2015, **39**, 881–890.
48 E. M. Agency, Background review for cyclodextrins used as excipients, https://www.ema.europa.eu/en/documents/report/background-review-cyclodextrins-used-excipients-context-revision-guideline-excipients-label-package_en.pdf.